

# Interaction of Convective Organisation with Monsoon Precipitation, Atmosphere, Surface and Sea: the 2016 INCOMPASS field campaign in India

A. G. Turner<sup>1,2,\*</sup>, G. S. Bhat<sup>3,4</sup>, G. M. Martin<sup>5</sup>, D. J. Parker<sup>6</sup>, C. M. Taylor<sup>7,8</sup>, A. K. Mitra<sup>9</sup>, S. N. Tripathi<sup>10,11</sup>, S. Milton<sup>5</sup>, E. N. Rajagopal<sup>9</sup>, J. G. Evans<sup>7</sup>, R. Morrison<sup>7</sup>, S. Pattnaik<sup>12</sup>, M. Sekhar<sup>13</sup>, B. K. Bhattacharya<sup>14</sup>, R. Madan<sup>15</sup>, Mrudula Govindankutty<sup>16</sup>, J. K. Fletcher<sup>6</sup>, P. D. Willetts<sup>6</sup>, A. Menon<sup>1,2</sup>, J. H. Marsham<sup>6,2</sup>, and the INCOMPASS team [K. M. R. Hunt<sup>1,2</sup>, T. Chakraborty<sup>11</sup>, G. George<sup>10</sup>, M. Krishnan<sup>10</sup>, C. Sarangi<sup>10</sup>, D. Belušić<sup>7,17</sup>, L. Garcia-Carreras<sup>6,18</sup>, M. Brooks<sup>5</sup>, S. Webster<sup>5</sup>, J. K. Brooke<sup>5</sup>, C. Fox<sup>5</sup>, R. C. Harlow<sup>5</sup>, J. M. Langridge<sup>5</sup>, A. Jayakumar<sup>9</sup>, S. J. Böing<sup>6</sup>, O. Halliday<sup>6</sup>, J. Bowles<sup>5</sup>, J. Kent<sup>5</sup>, D. O'Sullivan<sup>5</sup>, A. Wilson<sup>5</sup>, C. Woods<sup>5</sup>, S. Rogers<sup>5</sup>, R. Smout-Day<sup>5</sup>, D. Tiddeman<sup>5</sup>, D. Desai<sup>14,19</sup>, R. Nigam<sup>14</sup>, S. Paleri<sup>3</sup>, A. Sattar<sup>20</sup>, M. Smith<sup>21</sup>, D. Anderson<sup>21</sup>, S. Bauguitte<sup>21</sup>, R. Carling<sup>21</sup>, C. Chan<sup>21</sup>, S. Devereau<sup>21</sup>, G. Gratton<sup>21</sup>, D. MacLeod<sup>21</sup>, G. Nott<sup>21</sup>, M. Pickering<sup>21</sup>, H. Price<sup>21</sup>, S. Rastall<sup>21</sup>, C. Reed<sup>21</sup>, J. Trembath<sup>21</sup>, A. Woolley<sup>21</sup>, A. Volonté<sup>1,2</sup> and B. New]<sup>1</sup>

<sup>1</sup>Department of Meteorology, University of Reading, Reading, UK

<sup>2</sup>National Centre for Atmospheric Science, UK

<sup>3</sup>Centre for Atmospheric and Oceanic Sciences, Indian Institute of Science, Bengaluru, India

<sup>4</sup>Divecha Centre for Climate Change, Indian Institute of Science, Bengaluru, India

\*Correspondence Andrew G. Turner, Department of Meteorology, University of Reading, PO Box 243, Reading, RG6 6BB, UK Email: [a.g.turner@reading.ac.uk](mailto:a.g.turner@reading.ac.uk)

## Funding information

Natural Environment Research Council, Grant Numbers: NE/L01386X/1, NE/L013843/1 and NE/L013819/1; Ministry of Earth Sciences, Monsoon Mission; Royal Society Wolfson Research Merit Award; BEIS/Defra, Met Office Hadley Centre Climate Programme: GA1101

## Abstract

The INCOMPASS field campaign combines airborne and ground measurements of the 2016 Indian monsoon, towards the ultimate goal of better predicting monsoon rainfall. The monsoon supplies the majority of water in South Asia, but forecasting from days to the season ahead is limited by large, rapidly developing errors in model parametrizations. The lack of detailed observations prevents thorough understanding of the monsoon circulation and its interaction with the land surface: a process governed by boundary-layer and convective-cloud dynamics.

INCOMPASS used the UK Facility for Airborne Atmospheric Measurements (FAAM) BAe-146 aircraft for the first project of this scale in India, to accrue almost 100 hours of observations in June and July 2016. Flights from Lucknow in the northern plains sampled the dramatic contrast in surface and boundary layer structures between dry desert air in the west and the humid environment over the northern Bay of Bengal. These flights were repeated in pre-monsoon and monsoon conditions. Flights from a second base at Bengaluru in southern India measured atmospheric contrasts from the Arabian Sea, over the Western Ghats

This article has been accepted for publication and undergone full peer review but has not been through the copyediting, typesetting, pagination and proofreading process, which may lead to differences between this version and the Version of Record. Please cite this article as doi: 10.1002/qj.3633

mountains, to the rain shadow of southeast India and the south Bay of Bengal. Flight planning was aided by forecasts from bespoke 4km convection-permitting limited-area models at the Met Office and India's NCMRWF.

On the ground, INCOMPASS installed eddy-covariance flux towers on a range of surface types, to provide detailed measurements of surface fluxes and their modulation by diurnal and seasonal cycles. These data will be used to better quantify the impacts of the atmosphere on the land surface, and vice versa. INCOMPASS also installed ground instrumentation supersites at Kanpur and Bhubaneswar.

Here we motivate and describe the INCOMPASS field campaign. We use examples from two flights to illustrate contrasts in atmospheric structure, in particular the retreating mid-level dry intrusion during the monsoon onset.

### Keywords

Indian monsoon, INCOMPASS, field campaign, observations, systematic model bias, surface fluxes, tropical convection

## 1 Introduction and motivation

The monsoon supplies more than 80% of annual rainfall to more than a billion people in India and the surrounding region between June and September. The agrarian nature of large portions of Indian society, coupled with the growing population and developing economy, lead to ever-increasing demands for water; any variations in the monsoon on time scales of days to decades into the future can therefore have large impacts. A monsoon drought in July of 2002, for example, led to significantly reduced crop yields and economic damage (Gadgil and Gadgil, 2006; Challinor et al., 2006). Despite its importance to India, forecasting the monsoon from the medium range to the season ahead remains unreliable, and large biases are present in climate models (Turner and Annamalai, 2012; Sperber et al., 2013). Errors develop rapidly in numerical weather prediction (NWP) and climate models alike (Martin et al., 2010), suggesting that poor parametrizations and lack of process understanding are to blame. We aim to contribute to efforts to solving these problems through analysis of data from the INCOMPASS (Interaction of Monsoon Precipitation and Convective Organisation, Atmosphere, Surface and Sea) field campaign of 2016.

The physics of interactions between the surface, boundary layer and convection remain unclear and require detailed modelling and observations of land-atmosphere interactions and convection. Convective parametrizations, the primary source of modelled rainfall in the tropics, are associated with known errors in rainfall amount, frequency and timing of the diurnal cycle (e.g., Stirling and Stratton, 2012; Martin et al., 2017). Since convection is intimately linked through cloud heating and radiative feedbacks to the tropical circulation, both for the monsoon (Sperber et al., 2013) and more generally, the issue has been highlighted as a Grand Challenge by the World Climate Research Programme.

The monsoon is formed in response to the large-scale meridional tropospheric temperature gradient that develops during springtime (e.g., Xavier et al., 2007), at its heart due to the contrasting heat capacity between land and ocean and consequent differential fluxes of sensible heat (or alternatively, as a landward extension of the intertropical convergence zone (ITCZ) as in Gadgil, 2018). This leads to a large-scale overturning circulation and advection of moisture from across the Indian Ocean towards India.

Establishment of the monsoon is aided by sensible heating over the Tibetan Plateau (Li and Yanai, 1996), but the Himalayas and Hindu Kush are also important in blocking the flow. These steep features separate dry, low moist-static energy mid-latitude air from the moist tropical flow (Boos and Kuang, 2010; Molnar et al., 2010). Elsewhere in India, orographic enhancement also serves to bring significant rains to the Western Ghats mountains on the west coast of the southern peninsula, an aspect explored in detail using INCOMPASS field campaign data (Fletcher et al., 2019). Figure 1 shows the significant orography to the north and west of India and the Western Ghats over the southern peninsula.

In addition to the complex orography, a variety of surface types are present, ranging from the dry Thar desert of north-west India to the forested regions of the north-east coast. Between these extremes lies the Ganges river basin in the northern plains, home to India's largest population density and major agricultural production. As Figure 1 shows, the northern plains region of India features extensive irrigation practices, often drawing water from subsurface aquifers in addition to canals distributing water from the Ganges itself.

The monsoon onset begins with the reversal of the tropospheric temperature gradient (Xavier et al., 2007), typically on or around 1 June in the southern Indian state of Kerala. Rather than raining over India in a homogeneous manner, the monsoon progresses north-westwards across India over several weeks, its arrival at each location being critical for commencement of the crop-growing season. The monsoon finally arrives in the northwest near the border with Pakistan in mid-July, the region thus undergoing a significantly shorter wet season.

Figure 2a-c demonstrates the space-time inhomogeneity in the monsoon rains during the onset phase, based on long-term daily data. Two distinct gradients are apparent. Firstly, a gradient from wet north-east India to the dry northwest is seen to evolve in time as the onset progresses between mid-May and mid-July. Rainfall in the north-east peninsula is also aided by monsoon depressions, a type of cyclonic storm propagating north-westward from the Bay of Bengal, parallel to the Himalayas and along the axis of the monsoon trough (region of low mean-sea-level pressure shown in Figure 1); see Hunt et al. (2016a) for a thorough assessment. Secondly, a gradient quickly becomes established in the southern peninsula from the heavy rains over the Western Ghats to a drier rain-shadow region in south-east India, in the lee of the orography. As we will describe, sampling these two gradients in space and time was a key focus of the INCOMPASS field campaign.

A consequence of the spatio-temporal evolution of the Indian monsoon is the response of the surface to the rains. Figure 2d-f shows climatological satellite-derived surface soil moisture across India for the same dates as above. The rainfall distribution is clearly reflected in the

soil moisture, but there is also the suggestion of high soil moisture fractions in northern India prior to the onset of rains, likely related to irrigation practices. The importance of such soil moisture patterns in their control of whether surface fluxes are dominated by sensible or latent heat, and the subsequent impact on the boundary layer and cloud development are key areas of interest for INCOMPASS.

Analysis of the long-term observational record under INCOMPASS has already attempted to explain the north-westward progression of the monsoon onset as a battle between moist tropical lower-tropospheric air and a retreating mid-tropospheric dry intrusion that emanates from the northwest (Parker et al., 2016). The dry intrusion is shown to be eroded progressively from below and from the south; observations (Parker et al., 2016), and subsequent initialized coupled-model analysis (Menon et al., 2018), suggest that moistening of the free troposphere by detraining shallow and congestus convection near the freezing level leads the way to subsequent development of deep convection and advancement of the monsoon. The transition between shallow and deep convection is a notoriously difficult problem, with the cumulus congestus phase particularly difficult to parametrize as it detrains moisture to the free troposphere and primes the atmosphere for deep convection (Mapes and Zuidema, 1996; Parsons et al., 2000).

What is not well understood is how the land surface feeds back on the progression of the monsoon through its seasonal cycle, and on monsoon variability. It has been suggested that moistening of the soil ahead of the monsoon progression line, by light rains from the anvil of deep convective clouds, helps further the north-westward progression (Krishnamurti et al., 2012). But precisely how do pre-monsoon storms that moisten the surface help aid the development of deep convection? More generally, do soil moisture patterns arising either from antecedent rains or irrigation practices lead to the development of storms as observed in the West African monsoon (Taylor et al., 2011)?

An overview of previous field experiments in India has been given by Bhat and Narasimha (2007). In particular, much emphasis has been placed on the role of air-sea interaction and coupled processes, e.g., in the Bay of Bengal Monsoon Experiment (BOBMEX; Bhat et al., 2001). However, there is a distinct lack of observations particularly related to the land surface and its role in driving convection over India. While Vernekar et al. (2003) gathered some evidence of interactions between vegetation and the boundary layer in Gujarat in the Land Surface PRocesses Experiment (LASPEX), the paucity of surface flux measurements (particularly of latent heat) collocated with meteorology prevents an accurate assessment of the performance of land surface models, their parametrizations, and their behaviour when incorporated in full GCMs. Meanwhile in the troposphere, a poor understanding of how convection and the circulation really interact prevents the development of refined convective parametrizations, limiting model improvement. Since convective parametrizations will be needed in weather and climate prediction models for years to come, it is essential that efforts are focused on improving these parametrizations.

The overall goal of INCOMPASS is to better understand how an air parcel is modified as it travels toward India, crossing coastlines, mountains and a variety of land surface types and soil moisture patterns en route. This leads to the key science questions of INCOMPASS:

1. How are the characteristics of monsoon rainfall on sub-daily to intraseasonal time scales influenced by surface, thermodynamic and dynamic forcing, as monsoon air moves from the ocean inland and across India?
2. How do land-surface properties interact with the monsoon on hourly to monthly time scales and from kilometre to continental spatial scales?
3. What is the role of the land surface in the progression of the monsoon during its onset, and in monsoon variability, and can its understanding aid monsoon prediction?
4. How do convection and boundary layer behaviour on sub-daily time scales influence rainfall variability on intraseasonal and seasonal scales, in the real monsoon system and in models?

Through INCOMPASS, we will begin to answer these questions using observations and modelling from the field campaign in the monsoon of 2016. As we will describe, an airborne and ground observational campaign took place between May and July 2016, jointly funded by the Natural Environment Research Council (NERC) in the UK and Ministry of Earth Sciences (MoES) in India under the *Drivers of Variability in the South Asian Monsoon* programme. Airborne and ground observations, chiefly consisting of data from research flights on the Facility for Airborne Atmospheric Measurement (FAAM) Atmospheric Research Aircraft and an array of new surface flux towers, respectively, are supported by dedicated forecasting and case-study modelling.

This paper will outline the design of the INCOMPASS field campaign and catalogue the flights performed and instruments installed. Other related works will discuss the first results from the network of eddy-covariance flux towers installed by INCOMPASS (Bhat et al., 2019) and a detailed description of the thermodynamic and dynamic structure of the atmosphere associated with the portion of our field campaign in southern India (Fletcher et al., 2019). In addition to describing the INCOMPASS field campaign, in this study we will use airborne, ground and remote-sensing data to test a hypothesis suggested by Parker et al. (2016) on the evolution of the dry intrusion during the progression of the monsoon onset in 2016.

Section 2 describes the aircraft component of the field campaign, including the design of the flights, a description of the aircraft employed, its instrumentation, as well as details of the forecast models used in flight planning. Section 3 outlines the network of flux towers and other instrumentation installed by INCOMPASS, as well as an intensive observing period of radiosonde launches from Kanpur, northern India; in addition other data made available by the India Meteorological Department are listed. In Section 4, we use excerpts from INCOMPASS flight data to track the progression of monsoon rains across India in 2016 and test the interaction of the mid-level dry-air intrusion with moist air from the tropics. Finally, conclusions are drawn in Section 5 with an outlook to key related works and future plans.

## 2 The INCOMPASS 2016 aircraft campaign

A unique and key component to the INCOMPASS field campaign is a detachment of the FAAM Atmospheric Research Aircraft to India between May and July 2016. Here we describe the aircraft, our chosen operating bases in India, with justification, and the flights performed. We also briefly describe the aircraft instrumentation and forecast modelling used in support of the aircraft campaign.

## 2.1 The Atmospheric Research Aircraft

The UK FAAM Atmospheric Research Aircraft (aircraft hereafter) is owned by NERC, having originally been brought into service jointly with the UK Met Office. The aircraft is a modified BAe-146-301 passenger aircraft that is operated for FAAM by Airtask Ltd. (known as DirectFlight Ltd. in 2016). The maximum endurance of the aircraft is around 5 hours (although airport altitude, payload, and high operating temperatures encountered in India can reduce this), while the operational ceiling altitude is 35000 ft (about 10700m). The standard science speed and pitch angle were 200 knots indicated airspeed ( $\approx 100\text{ms}^{-1}$ ) and  $+4.5^\circ$ , respectively, with a minimum safe altitude down to 50 ft (15m) over the sea, although typically double this at 100 ft for straight and level runs, or around 600 ft (183m) over land. For more detail, see [www.faam.ac.uk](http://www.faam.ac.uk). Use of the aircraft was shared with a sister project (SWAAMI, South West Asia Aerosol Monsoon Interactions; Brooks et al., 2019), also funded under the joint NERC-MoES programme.

## 2.2 Choice of airbases and operating period

When designing the flight operations of INCOMPASS we kept in mind the need to sample two distinct sets of spatial gradients formed across India during the monsoon, as motivated in Section 1:

- The precipitation gradient from wet north-east India to dry north-west India and the evolution of this gradient from the pre-monsoon through the monsoon onset;
- The zonal precipitation gradient over southern peninsular India, crossing the Arabian Sea coast, the Western Ghats mountains, the rain shadow of south-east India and the Bay of Bengal coast.

After considering the distance between these locations and the airports permitting our operation, two bases were chosen. A northern base in Lucknow (Uttar Pradesh), central to the northern plains, would allow flights both to the southeast, passing the Bay of Bengal coast near Bhubaneswar, and to the west, reaching Jodhpur and the Thar desert. Flights could be made from Lucknow in either direction with a return to the airbase without refuelling. A southern base was established in Bengaluru (Bangalore) at the former international airport, known as HAL or Hindustan Airport. Being central to the southern peninsula, flights from Bengaluru would allow sampling across the Western Ghats and Arabian Sea in the west, or over the rain shadow and into the Bay of Bengal towards the southeast.

The need to sample gradients in northern India, and their evolution as the monsoon progresses and the surface moistens, suggested we must begin flights from Lucknow

sufficiently early in the season in order to capture the *pre-monsoon* period; in the pre-monsoon there is little overall rainfall in the north, although with a strong gradient from the dry Thar desert to the north-east coast (see Figure 2a). We would return to Lucknow later in the season, once the monsoon becomes established there and soils have moistened further west (Figure 2c,f). We therefore operated flights from Lucknow in both early June and in July. Due to bureaucratic reasons, science flights were not able to commence from Lucknow until 11 June 2016 (see Table 1), much later than hoped. Fortunately (from a scientific perspective), the 2016 monsoon onset in northern India was delayed, not reaching the vicinity of Lucknow until 21 June. This allowed us to sample east-west gradients in the atmospheric structure in northern India before the monsoon had become fully established, and then again later in the season.

In the southern peninsula, fortunately the west-to-east gradient in rainfall becomes established early in the monsoon and is a robust feature, owing to the consistency of the westerly winds from the Somali Jet and rains associated with orographic enhancement. Thus we were able to plan our flight period of one week in Bengaluru well in advance, confident that the climatological features of the monsoon would be present. Flights from Bengaluru took place in late June.

### 2.3 Flights performed

Following the overall timing of the flight campaign outlined above, a list of the flights performed from the two airports and their brief scientific objectives are given in Table 1 and described further below. A map of the flights undertaken is shown in Figure 3, grouped by the main purpose in each case. The majority of flights were designed to sample the manifestation of climatological contrasts in the monsoon during the 2016 season and their evolution.

To the west from Lucknow, sorties flew towards Jodhpur and over the Thar desert, into the heat low region of the monsoon (B956, B968-B970, B972, B973 & B976). Meanwhile, flights to the south-east of Lucknow were in the direction of Bhubaneswar and over India's north-east coast to the Bay of Bengal (B957, B971 & B975). Taken together, these northern flights allow the sampling of land-atmosphere coupling; assessing contrasts in cloud and boundary layer structure as the surface beneath changes from the dry desert in the west, along the Ganges basin towards the forests of the northeast coast, as well as the coastal transition. En route, the impacts of antecedent soil moisture or irrigation patterns on the atmosphere could be assessed (e.g., in the study of Barton et al., 2019). Flights from Lucknow were possible both prior to (2 flights: B956 & B957) and after the onset in northern India (8 flights: B968-B973, B975 & B976). Work is currently being undertaken to analyse the output from these flight data (not shown). For the allied SWAMI project that made use of the aircraft, flights over northern India were ideal for sampling desert dust as well as anthropogenic aerosols emanating from megacities such as Delhi, and biomass burning (e.g., as in Brooks et al., 2019).

In southern India, flights were performed to the west and east, measuring transitions across the Arabian Sea coast/Western Ghats and Bay of Bengal coast, respectively. Six flights to the

west from Bengaluru were performed during this portion of the mission (B959, B961-B965), with take-offs at different times of day in order to sample atmospheric structure and convective initiation through the diurnal cycle. These flights are the subject of a further work in this issue (Fletcher et al., 2019).

Two flights to the southeast from Bengaluru (B960 & B966) sampled the rain shadow region in the lee of the Western Ghats. One of these flights (B966, 27 June) also performed an overpass of the Council of Scientific and Industrial Research National Institute of Oceanography vessel RV Sindhu Sadhana that was undertaking a survey as part of the BoBBLE field campaign (Vinayachandran et al., 2018); future analysis together with data from this flight will allow for collocated vertical profiles of the atmosphere and ocean and related air-sea interactions during that day of 2016.

Other than the diurnal sampling during westward flights from Bengaluru (B959, B961-B965), flight take-offs were usually in the morning (see Table 1) in order that surface-induced structures in the boundary layer could be sampled on the return leg, once the boundary layer is more developed, and, pragmatically, so that cabin temperatures could be kept cool enough prior to take off.

Longitude-height cross sections of all flights except the north-south transit flights (B958 & B967) are shown in Figure 4. Each of these flights followed a broadly similar strategy. An initial high-level run surveyed the atmospheric structure beneath. The transit altitude for this run was planned as a couple of thousand feet above the likely top of the uppermost cloud and aerosol layers. This allowed the on-board downward-pointing lidar (see details in Section 2.5) to take adequate measurements of any cloud layers below it. Ascents at the beginning and end of high-level portions were performed at a rate of 1000 ft/min, sufficiently slow to enable scientific sampling of pseudo-in situ parameters (and, for example, the construction of tephigrams). Science flying speed once level was  $100\text{ms}^{-1}$ . The return portion of each flight was performed at low levels if permitted by weather conditions (sufficient low-level visibility, particularly in the vicinity of orography) and air-traffic restrictions. This low-level was a minimum altitude of 600ft above ground level or 100ft above the sea surface. Under low visibility conditions (or nighttime), low-level runs were performed at higher altitude, usually 500 ft above the sea and 2000 ft above the land. The low-level portions allowed for accurate transect measurements of land (or sea) surface temperature, estimation of fluxes at flight level, and observations of heterogeneity in the boundary layer response to surface types such as patterns of soil moisture or irrigation, and also for sampling of the subcloud layer. Some flights contain additional ascent or descent portions, allowing for additional vertical sampling to be performed of any cloud and aerosol layers, as well as standard meteorological parameters. The reader may note some additional ascent before the landing procedure in Figure 4, required since the final approach to an airport occurs on a defined glide slope.

In addition to the near-zonal transects across northern and southern India, the relocation between airbases required meridional transit flights between Lucknow and Bengaluru (B958, 13 June) and the return (B967, 28 June). These featured a long, level run at around 400hPa; in addition, near the half-way point (around 20°N close to Nagpur), the transit flights gathered

descending and ascending atmospheric profiles down to 1500 ft (in the absence of dropsondes). Some analysis of observations from these flights will be presented in Section 4.

While the decision to fly a pre-planned climatological transect could be made if the weather conditions were right for measuring a particular spatial contrast (see our forecast methodology in Section 2.4), other flights were designed in response to impending synoptic events that could occur at any time. One such example is monsoon depressions, which can occur around 3-6 times per summer and propagate in a north-westward direction along the monsoon trough (Saha et al., 1981). Poor simulation of monsoon depressions is thought to be a key factor in the dry rainfall biases prevalent in the Fifth Coupled Model Intercomparison Project (CMIP5) models (Sperber et al., 2013). Since depressions are associated with large amounts of rainfall in northern and central India (Hunt et al., 2016a,b), a more detailed dynamic and thermodynamic understanding of the processes involved in a depression would be valuable. Fortunately, one such monsoon depression occurred during INCOMPASS, and a flight south-westwards from Lucknow was devised to sample this depression at low and high altitudes (flight B974, 7 July 2016, see Table 1). Flight B974 represents the first flight through a fully formed monsoon depression since that of July 1979 during the Monsoon Experiment (MONEX) campaign (as covered in Houze and Churchill, 1987), and the first ever depression flight, to our knowledge, over land. Separate works covering detailed observational and model analysis of the July 2016 depression are being prepared for this Special Collection.

## 2.4 Forecast modelling in support of the flight campaign

Due to air traffic control restrictions, flight plans had to be filed by noon two days before an intended flight. There was therefore a fundamental requirement for accurate forecasts of weather conditions. Idealised flight plans were prepared in advance such that the most suitable plan could be selected, amended and filed with the authorities according to the forecast conditions and scientific goals. Flight planning during the 2016 campaign was aided greatly by the team's experience of a mock or *dry-run* forecasting and flight-planning exercise carried out one year earlier (the subject of Willetts et al., 2017b). In that exercise, forecast briefings were held each morning during a month of the 2015 monsoon onset period, using all available forecasts. The dry-run methodology of Willetts et al. (2017b) made for efficient flight planning in the 2016 flight campaign itself.

The chief forecasting tool was the Met Office Unified Model (MetUM) and its derivatives. The operational version in use in 2016 was the GA6.1/GL6.1 science configuration operating at a horizontal resolution of N768 ( $\approx 17\text{km}$ ) with 70 vertical levels. GA6.1 is the science configuration for the MetUM global atmosphere including parametrized deep and shallow convection, and GL6.1 defines the Joint UK Land Environment Simulator (JULES) global land science configuration; both are described in Walters et al. (2017). The operational global analysis-forecast cycle produces analyses at 00Z, 06Z, 12Z and 18Z, and 7-day (168-hour) forecasts are run twice a day from the 00Z and 12Z analyses.

Recognizing that models featuring parametrized convection typically perform poorly in the tropics, particularly in their representation of the diurnal cycle of convection, a bespoke limited area model (LAM) was developed (covering a domain of  $5 - 35^{\circ}\text{N}$ ,  $50 - 100^{\circ}\text{E}$ ). This LAM operated at a resolution of 4.4km and represented convection explicitly, i.e. the convection parametrization was completely switched off. The LAM was initialised using the interpolated global model analysis flow fields and forced at the lateral boundaries from large-scale conditions generated every hour by the global model.

Further forecast products were provided by global and regional versions of the NCUM (NCMRWF Unified Model) implemented at India's National Centre for Medium Range Weather Forecasting (NCMRWF). Outputs from global 17 km, regional 4.0 km and 1.5 km versions of the model were used on a daily basis for flight planning. Example outputs from these models for day-2 rainfall forecasts are shown in Figure 5. The 4 km and 1.5 km regional versions use explicit convection schemes (Mamgain et al., 2018), compared to the parametrized convection used in the 17 km global model. The 1.5 km configuration also uses the moisture conservation scheme of Aranami et al. (2015). This attempts to mitigate the inherent non-conservation of semi-Lagrangian advection that arises due to the strong localised horizontal moisture gradients in a model with resolved convection.

Analysis of traditional parametrized and convection-permitting models has shown that permitting convection leads to improvements in the timing of the diurnal cycle of convection in India during monsoon model experiments (Willetts et al., 2017a). Experience during the field campaign suggested that, while the 17 and 4.4km models featured the same synoptic wind and surface pressure patterns, the diurnal cycles were very different: precipitation being forecast too early in the global parametrized model and perhaps too late in the convection-permitting model. The NCUM forecast example presented in Figure 5 shows typical active monsoon conditions in the Indo-Gangetic plains. The NCUM regional models show much more detailed rainfall patterns compared to the 17 km global model forecasts. However, overestimation of rainfall in the regional model is a known issue and is primarily dominated by deep convection and higher maximum vertical velocities than in the global model (e.g., Martin et al., 2019). The global model has problems related to the location of maximum rainfall (associated with movement of the monsoon low), whereas the regional model better captures its intensity and location.

Further details of these models and their use to support the INCOMPASS field campaign are given in Martin et al. (2019), while their performance at forecasting the Indian monsoon in 2016 is the subject of further works in this Special Collection (Jayakumar et al., 2019; Sandeep et al., 2019).

Forecast products were sent via automatic upload to an operations room near the airport base. During flights, mission scientists were updated with more recent forecast information and images from India's Kalpana geostationary satellite and Meteosat 7; this helped to inform decisions about the flight ahead, for example if severe weather needed to be avoided.

## 2.5 Atmospheric Research Aircraft instrumentation

Here we briefly describe the instrumentation fitted to the aircraft. A fuller description can be found in (e.g.) Renfrew et al. (2009) or at [www.faam.ac.uk](http://www.faam.ac.uk).

### 2.5.1 Core instrumentation for in situ measurement

Basic information on the aircraft's position, velocity and attitude (angle-of-attack) is provided by a GPS-aided inertial navigation system. A five-hole turbulence probe mounted on the aircraft nose is used in conjunction with the navigation system and static pressure ports (pitot tubes) to also determine zonal, meridional and vertical wind velocities as well as high-frequency turbulence measurements (at 32Hz; Petersen and Renfrew, 2009). An Aircraft Integrated Meteorological Measurement System (AIMMS-20) was also used to make measurements of the 3D-wind components. In addition to altitude provided by the satellite navigation system, a radar altimeter is used to provide more accurate measurements when close to the surface, with accuracies of 2% (below 2500ft) and 3% (2500-5000ft) but increasing error at higher altitudes (Renfrew et al., 2009).

Temperature measurements include a Rosemount/Goodrich 102AL/102BL platinum-resistance immersion thermometer mounted near the aircraft nose to provide de-iced and non-deiced true air temperature, to an accuracy of 0.3°C (Renfrew et al., 2009). A variety of humidity measurements are available, including the water-vapour sensing system version two (WVSS-II). This instrument is a near-infrared tunable diode absorption spectrometer and measures atmospheric water vapour to an accuracy of 5%. A detailed comparison of the measurement performance of all five hygrometers fitted to the aircraft is described in Vance et al. (2015). The WVSS-II has been shown to give more precise humidity measurements and with a more rapid response to change in all synoptic conditions. Further measurements of liquid water content are provided by a Johnson-Williams probe using a heated wire resistance bridge. Finally, upward and downward-pointing modified Epply pyranometers were used to measure up- and downwelling shortwave irradiance.

### 2.5.2 Remote sensing instruments

During other observational campaigns, the aircraft is able to launch dropsondes to measure atmospheric profiles beneath the aircraft during straight-and-level runs at high altitude. Unfortunately, due to air traffic control stipulations, the use of dropsondes was not permitted during INCOMPASS.

However, vertical atmospheric profiles could be obtained from a nadir-facing Leosphere ALS450 elastic backscatter lidar operating at a wavelength of 355nm (Marenco et al., 2014). The lidar measures range-corrected signal and cloud-top height, and with additional processing aerosol extinction coefficient and aerosol optical depth (Marenco et al., 2011). This enables the position of atmospheric layers below the aircraft to be determined. In-flight monitoring of the lidar output provided information on the height of the boundary layer.

In addition to the core radiation instrumentation, the Spectral Hemispheric Irradiance MeasurementS (SHIMS) instrument measured spectrally resolved downwelling and upwelling irradiance from 0.3 to 1.7 $\mu$ m (Ryder et al., 2015). Remote sensing of surface

temperatures was provided by two instruments. Firstly, the Heimann KT 19.82 radiometer measures upwelling infrared radiation over the spectral range of 8 to 14 $\mu\text{m}$  at 4Hz. Secondly, the Airborne Research Interferometer Evaluation System (ARIES) is a nadir and zenith-pointing infrared interferometer measuring radiances at a resolution of 1cm $^{-1}$  between 550cm $^{-1}$  and 3000cm $^{-1}$  (Wilson et al., 1999). Using the method of Newman et al. (2005), and adapted from Fielder and Bakan (1997), a retrieval of surface temperature and emissivity can be achieved under clear-sky conditions. As with other on-board instrumentation, multiple sampling techniques allow for cross-calibration and operational redundancy in the event of instrument error.

### 2.5.3 Other instruments

Although not the subject of the INCOMPASS campaign, aerosol measurements include scattering at three wavelengths from a TSI 3563 nephelometer, aerosol absorption at 565nm from the Particle Soot Absorption Photometer (PSAP) and accumulation mode aerosol size distribution from a wing-mounted Passive Cavity Aerosol Spectrometer Probe (PCASP). In addition, a Cloud Droplet Probe (CDP) was deployed for the measurement of coarse mode aerosol as well as cloud droplet number and size distribution. A Cloud Imaging Probe (CIP15) was used to measure larger precipitation-sized particles. Finally, an Aerosol Mass Spectrometer (AMS) and Single Particle Soot Photometer (SP2) owned by University of Manchester allow for in-situ sampling of aerosol mass concentration, and quantification of refractory black carbon (rBC) mass loadings and number concentrations (e.g., Stephens et al., 2003; Liu et al., 2010). Such measurements were used by SWAAMI (Brooks et al., 2019) to study aerosol composition during the pre- and mature monsoon periods.

Due to legal restrictions forbidding aerial photography in India, the aircraft's Imaging Infrared Radiometer (IIR) used for live multi-directional cameras could not be fitted during the INCOMPASS mission.

## 3 Ground and upper-air instrumentation

While a unique aspect to INCOMPASS is the 2016 flight campaign described above, of equal value are ground-based measurements, some of which are enduring beyond the lifetime of INCOMPASS. These comprise surface flux towers, upper-air stations, microwave radiometers and other instrumentation, to be described in the following section. The reasoning behind the installation of these instruments and likely uses are given below.

### 3.1 Eddy covariance flux towers

The main ground instrumentation implemented by INCOMPASS is a series of eight eddy covariance flux towers spread across the country. Flux tower locations (listed in Table 2 and shown in Figure 6) were chosen to facilitate mapping across various hydroclimatic zones of India and different agricultural types (a brief description of the surrounding surface is found in the table; for more detail see Bhat et al., 2019).

Four of the towers (Berambadi, Chandan, Nawagam and Pusa) consisted of augmenting existing agro-meteorological (AMS) stations operated by the Indian Space Research Organisation (ISRO) with fast-response eddy covariance systems, while the remaining four (Bengaluru, Bhubaneswar, Dharwad and Kanpur) were new installations. The eddy covariance technique offers improvement over earlier Bowen ratio methods since fluxes of moisture, heat or atmospheric gases can be measured directly as part of vertical turbulent motions, with a typical frequency of 20Hz. The former sites would allow direct comparison of the eddy covariance technique with results from slower, older sensors in their estimates of the surface energy budget. The AMS data measurements consist of four-component radiation, soil heat fluxes, soil moisture and rainfall, as well as air temperature, relative humidity, wind speed and direction at three heights, sampled at 5-minute intervals and averaged over 30 minutes. The eddy covariance instrumentation supplements this with latent heat flux, sensible heat flux, friction velocity ( $u^*$ ) and net carbon dioxide ecosystem exchange (NEE). At Berambadi, Dharwad and Kanpur, the Centre for Ecology and Hydrology (CEH) installed Licor gas analyser-based eddy-covariance flux systems (model LI7500A with Gill 3D sonic anemometers); systems at other sites were based on Campbell Scientific Inc. instrumentation (model EC150 with Campbell 3D sonic anemometer) and installed by IISc Bengaluru. Licor and Campbell EC systems are configured to sample at 10 and 20 Hz, respectively.

The EC systems at Berambadi, Dharwad and Kanpur are co-located with cosmic-ray sensors that provide continuous, area-averaged observations of near-surface (upper 0.05 to 0.2 m) volumetric soil water content ( $\text{m}^3 \text{m}^{-3}$ ) over an area of  $\approx 160\text{m}$  in radius (Zreda et al., 2012; Kohli et al., 2015). The intermediate spatial scale of cosmic-ray observations compared to other (e.g., point scale) measurement techniques is proving increasingly useful for the calibration and validation of remotely-sensed and modelled soil moisture data products (e.g., Evans et al., 2016; Montzka et al., 2017). The CRS sensors at these INCOMPASS flux tower sites form part of a wider soil moisture observation network that is being developed for various land cover types across India (<https://cosmos-india.org>).

While a detailed assessment of the diurnal cycle of surface fluxes is beyond the scope of this overview paper, an illustration of the large contrasts in surface flux partitioning across India during the mature monsoon is shown in Figure 7. Fluxes at two contrasting sites are shown: Jaisalmer (a semi-arid area in the Thar desert dominated by natural Sewan grass) and Samastipur (in the Indo-Gangetic Plains (IGP) surrounded by rice cultivation). The time period selected is August 2016, a month when the monsoon is well established over the entire sub-continent. The strong influence of solar heating on the diurnal variation of SH and LH is clear at both sites. SH dominates at Jaisalmer even during August whereas LH dominates at Samastipur, illustrating the east-west contrast in surface conditions arising from the monsoon pattern and surrounding land use. The standard deviations of SH and LH at Jaisalmer are more than double those at Samastipur. Scatter plots of LH versus SH (Figure 7d,e) exhibit two regimes at Jaisalmer; here, the soil is sandy, rain is less frequent and the overall influence of the monsoon is much less than at Samastipur. LH increases after rains but the surface energy budget becomes dominated by sensible heat. Meanwhile, standing water is the norm

in the rice fields of Samastipur, and evapotranspiration is energy rather than moisture limited, with LH dominant all the time.

The network of flux towers presented in INCOMPASS represents the first freely available quality-controlled flux dataset for India (Morrison et al., 2019b,a). Detailed findings based on flux sites across India are presented elsewhere in this Special Collection (Bhat et al., 2019). We will continue to use these data to assess the impact of the heterogeneous land surface in India on meteorology and vice versa, for example in the dry-down of the surface following active periods of monsoon rainfall or after the withdrawal of the monsoon as a whole; in addition, the flux data will be invaluable for understanding model biases in surface temperature and the surface energy budget in land surface models, both when used alone and incorporated into GCMs. While the flux tower installations took place in order to observe the 2016 monsoon, we anticipate these observations to continue for several years, potentially providing samples over around five or more seasonal cycles.

### 3.2 Supersites and other ground instrumentation

INCOMPASS established two *supersites* in the northern Indo-Gangetic plains of India, situated at partner institutes in Kanpur and Bhubaneswar, respectively.

Situated at IIT Kanpur, our first supersite is central to the northern plains, and thus mid-way along the longitudinal axis of the monsoon trough during the mature part of the season. The region features generally low-lying orography as part of the Ganges river basin, as well as significant portions of irrigated and rain-fed agriculture. We expect our measurements here to provide information on the evolution of the monsoon trough as part of the monsoon seasonal cycle as well as during monsoon intraseasonal variability or the passage of a monsoon depression.

The site itself is a semi-urban area on the outskirts of Kanpur city; while the flux tower described above is located around 1 km away on an area of semi-natural grassland within the boundaries of the campus, the majority of instruments are based at the IIT Kanpur airstrip. (The airstrip is used infrequently by a gliding club.) Instruments here include a Campbell Scientific lidar ceilometer CS135, installed on the roof of the airstrip control tower. The ceilometer provides a backscatter signal enabling the calculation of the height of cloud base (if any) every 20s, in addition to giving useful qualitative information regarding layering in the lower troposphere, for instance related to layers of differing aerosol composition. A HATPRO temperature and humidity-profiling microwave radiometer (MWR) manufactured by Radiometer Physics GmbH, Germany (Rose and Czekala, 2011) was also installed on the control tower. HATPRO data outputs include profiles of temperature and humidity (both relative humidity and water vapour density) up to 10 km height, integrated water vapour, cloud liquid water path and cloud base height. Finally, the same site was also used for radiosonde launches, as described in Section 3.3.

A second supersite was instituted at the new rural campus of IIT Bhubaneswar near to the eastern coast of Odisha state, adjacent to the Bay of Bengal. This location is an ideal

sampling point for observing the entrance to the monsoon trough, as moisture passes across the coast and up the IGP from the Bay of Bengal. Monsoon depressions also typically pass over this region as they cross the coast. In addition to the flux tower, a micro-rain radar (MRR), a Thies CLIMA optical disdrometer and a HATPRO MWR were also installed here. The METEK 24.1 GHz MRR provides profiles of drop-size distribution, rainrates, liquid water content and droplet falling velocity; the high sensitivity of this instrument allows detection at thresholds below the level of typical rain gauges.

Finally, a third microwave radiometer was installed at Bhopal in central India, in order to capture variations in meteorology associated with any monsoon depressions that make it inland.

We anticipate ongoing measurements from these instruments for several years.

### 3.3 Upper air data

INCOMPASS has access to radiosonde data from 19 upper-air stations spread across India, and operated by IMD. The locations of these launch sites are listed in Table 3 and shown in Figure 6. In addition to the regular ascents at 00Z and 12Z, INCOMPASS was able to supplement these at all 19 stations with additional measurements on the following dates:

- 7–10 July inclusive, at 06Z, 09Z & 18Z (coincident with the passage of a monsoon depression across central India);
- 4–6 August inclusive, at 06Z & 18Z;
- 26–30 September inclusive, at 06Z & 18Z.

During the observational campaign a total of 272 ascents were taken at each station. The sondes across these sites are a mixture of Chengfeng (Chinese), Jinyang (Korean) and GRAW (German) equipment.

In addition to the network of IMD radiosondes, INCOMPASS established a dedicated upper-air station at the IIT Kanpur supersite, for an intensive observing period (IOP) during July 2016 (location also listed in Table 3). The IIT Kanpur launches used Vaisala RS41 radiosondes, which combine humidity and temperature sensors and a global positioning system (GPS). Entire vertical profiles of relative humidity, temperature, pressure, wind speed and direction, and altitude, can be achieved with measurements taken every second. An assessment of the improved accuracy of these fourth-generation Vaisala sondes over their predecessors in the RS92 family can be found in Jensen et al. (2016). Radiosondes were released from the airstrip of IIT Kanpur, a sufficiently open area, to avoid surface interference in the launches. A Vaisala MW41 receiving station and CG31 portable antenna, both loaned from University of Reading, were housed in the airstrip's control tower. As far as possible, INCOMPASS tried to achieve 8 launches per day (every 3 hours) during the Kanpur IOP from 5–28 July 2016; the launch schedule achieved is shown in Figure 8, giving a total of 137 launches. Being central to the monsoon trough, the Kanpur IOP was able to capture the passage of a monsoon depression across the region (also the subject of flight B974 on 7 July 2016). George et al. (2018) have already used these data to examine the impacts of the

passing depression on cloud vertical structure and longwave/shortwave cloud radiative forcing.

Further work will use the Kanpur and other high-frequency radiosonde launches with flux tower output, for examining the impact of surface fluxes on atmospheric profiles, or in conjunction with flight data as additional inputs in observing system simulation experiments (OSSE; e.g., Errico et al., 2007). In OSSE, also known as data-denial experiments, NWP forecasts will be performed with the inclusion of additional observations in the assimilation scheme, to determine the impact of those new observations on the development of forecast errors.

### 3.4 IMD data supporting the field campaign

In addition to INCOMPASS airborne and ground measurements, the project was provided with access to the full range of data routinely collected by IMD for the duration of the 2016 field campaign. In addition to the radiosonde data described above, observational data were available from:

- About 1300 automatic rain-gauge (ARG) and 500 automatic weather station (AWS), and 550 surface observatory sites across India;
- 62 manually operated pilot balloon observatories using optical theodolites for tracking the balloon to measure wind data;
- 24 further RS/RW observatories in addition to the 19 stated in Table 3;
- 19 Doppler Weather Radar stations operating sporadically (manufacturers: Vaisala, Beijing Metstar, Gematronik, Bel);
- Outputs from India's Kalpana geostationary satellite system were also made available each half-hour.

## 4 Monsoon contrasts during the flight campaign

As a means of introducing some of the flight data collected during the INCOMPASS field campaign, in this section we analyse data from the two north-south transit flights (B958 & B967). We also use these data to provide supporting evidence from the 2016 season for the hypotheses of Parker et al. (2016) regarding the monsoon onset.

### 4.1 Contrasts at the surface

In order to outline the advance of the monsoon rains during the 2016 season between the two phases of flights, Figure 9 shows the accumulated rainfall since the beginning of the monsoon (nominally 1 June) and the date of each north/south transit flight (B958, north to south on 13 June; B967, south to north on 28 June 2016). The comparison between the climatological (expected) monsoon positions, and the IMD-declared positions in 2016 in Figure 9 demonstrates that by 13 June, the monsoon was delayed in its northwestward progression, reaching only around Nagpur. By 28 June, more complete coverage of India was achieved,

although the northern plains including the Lucknow area had only accumulated between 64–128mm by this stage.

To determine the impact on the land surface, the change in satellite-derived soil moisture between the two transit flights is shown in Figure 10a. Consistent with the advance of monsoon rains in a north and north-westward direction, soil moisture undergoes increases of 10–15% over much of eastern India and the northern plains (including the northern airport base of Lucknow). By the time of the return flight to Lucknow on 28 June 2016, regions of northwest India still featured dry soils, enabling the INCOMPASS mission to pursue its goals of sampling the effect of zonal contrasts in soil moisture on the overlying atmosphere.

Given the increase in soil moisture as the monsoon progresses, we can also infer the effects on partitioning of turbulent heat fluxes at the surface. Figure 10b shows observations of surface skin temperature ( $T_s$ ) and surface air temperature (at 2m,  $T_a$ ) from the AMRS2 satellite and ERA-Interim reanalysis, respectively. Large reductions of  $T_s$  (of order 10°C) are noted over much of India due to wetting of the soil and growth of vegetation, while  $T_a$  reduces by only 2–4°C. Since sensible heat ( $H$ ) is proportional to  $T_a - T_s$ , we can infer that sensible heat fluxes from the surface are declining as the monsoon progresses between the 13 June and 28 June periods.

## 4.2 Atmospheric contrasts

We use meridional sections roughly aligned to these north-to-south flights in the subsequent analysis to study the contrast in atmospheric structure as the monsoon of 2016 progresses. To examine the thermodynamic structure of the atmosphere, Figure 11 shows the equivalent potential temperature ( $\theta_e$ ) calculated from temperature and moisture outputs in ERA-Interim (Dee et al., 2011) and flight data (see Section 2.5).

Flight B958 consisted of ascent from take-off at Lucknow to an operating height ranging from 24–26 kft throughout the flight, heading approximately southward to Bengaluru. In order to gather additional vertical profiles, descent was made to an altitude of 460m (1500 ft) in the region of Nagpur, before returning to cruise altitude. Flight B967 repeated this route in reverse.

The south-to-north positive gradient in  $\theta_e$  near the surface features contributions from both moisture and temperature (not shown). The enhancement of this surface gradient on 28 June 2016 results from an increase in lower tropospheric specific humidity to values  $\approx 20\text{ g kg}^{-1}$  at 25°N. While ERA-Interim captures these general features, the B967 flight data suggest  $\theta_e$  is around 6K higher in the boundary layer at 20°N and beyond 25°N, mainly arising from higher humidity values (not shown).

The other main feature of Figure 11 is the region of low  $\theta_e$  in the mid-troposphere in both ERA-Interim and flight data, centred at 600hPa and most apparent in the early season on 13 June. This layer appears to be centred slightly higher in the vertical in the flight observations of the southern profile. Analysis of the temperature and moisture contributions to  $\theta_e$  determines this feature to arise from a layer of dry air (as low as  $\approx 2\text{ g kg}^{-1}$ ). In flight

observations for B958 (Figure 11a), the dry intrusion at 20°N is considerably drier, arising from lower specific humidity than in ERA-Interim (not shown); the vertical gradient in ERA-Interim is therefore too weak compared to observations. For both flight dates, the boundary layer  $\theta_e$  seems systematically too low.

Taken together with the progression of the monsoon shown in Figure 9, this dry air intrusion and its subsequent retreat northwards by 28 June is consistent with the mechanism proposed by Parker et al. (2016) whereby the dry air, originating over the north-west of the subcontinent, is eroded from beneath as the monsoon rains advance and moisten the free troposphere around the freezing level, aided by detrainment from shallow clouds (Menon et al., 2018).

To explore the differences between aircraft observations and ERA-Interim implied by  $\theta_e$ , we compare thermodynamic profiles over the centre of the transit flights (the vertical profiles near Nagpur at  $\approx 20^\circ\text{N}$ ) in radiosonde soundings, the flight profile and from ERA-Interim for both dates in Figure 12. The descent profile of the flight was chosen in each case since it is much smoother than the ascent. Immediately apparent is the higher temporal (and therefore vertical) resolution of the flight data. There is surprising agreement between the different data sources over the general vertical profile on both dates. On 13 June, the boundary layer is at a very consistent temperature in the flight and ERA-Interim model output, although the sonde profile is warmer by some margin. However this likely relates to its launch in the late afternoon compared to the other measurements. There are discrepancies aloft, with the dry intrusion in the flight observations (seen in the  $T_d$  lines) extending further up, and drier in parts compared to ERA-Interim, supporting the results of Figure 11a. (This is irrespective of whether the descending or ascending profiles from the aircraft are examined; not shown.) On 28 June, more extensive dry regions are found in the flight data over the 700–800hPa layer (green line), consistent with Figure 11b. However, without knowing the extent of this dry layer in the horizontal, it is difficult to determine whether a model error is present for ERA-Interim. A further outcome of this comparison, setting aside discrepancies likely arising from the time of day, is that the Nagpur radiosonde appears to match well the thermodynamic profile measured by the flights. If the high resolution sonde data were available, this would make a valuable input to assimilation systems if not already incorporated.

Finally, to explore spatial gradients in the thermodynamic structure in more detail, in Figure 13 we examine soundings from six upper-air stations that approximately follow the south-to-north flight paths between the two dates. These stations are: Bengaluru, Hyderabad, Nagpur, Bhopal, Gwalior and Lucknow (positions as indicated on Figure 9).

On both dates in Figure 13, there is a clear south-to-north gradient in atmospheric moisture, which deepens towards the south. By 28 June 2016, the profile is moister and deeper much further north. Near to Nagpur (third panel in each case) the profile is pseudoadiabatic up to the 500hPa level on 28 June, consistent with the northwestward propagation of the monsoon rains and gradual push of the deep moist profile northwards against the dry intrusion as in Parker et al. (2016). Thus we are confident that, at least in 2016, the northwesterly dry intrusion retreated as expected during progression of the monsoon onset.

Further work in INCOMPASS, together with use of the convection-permitting limited area model, will help determine whether the dry intrusion is eroded as part of a smooth progression or as a series of synoptic events that wax and wane (Volonté et al., 2019).

## 5 Summary

Given the large biases that have persisted for many years in simulations of the Indian monsoon in NWP and climate models, and the clear paucity of observations at the land surface with which to challenge and evaluate both land-surface models and GCMs, there was a clear need to gather detailed observations of the Indian monsoon. INCOMPASS set out to understand, at a fundamental level, how monsoon air is modified as it arrives at India and passes over a variety of surfaces modified by orography, soil moisture patterns, various types of land cover and irrigation practices.

In the INCOMPASS project, we devised and carried out a field campaign during the 2016 monsoon, based around a detachment of the FAAM Atmospheric Research Aircraft to India. INCOMPASS was the first such campaign using a foreign aircraft in India. Data from 22 research flights were used to measure the atmospheric structure across northern and southern India, with particular focus on how the boundary layer and convection may change over different surfaces. Recognising the lack of detailed measurements at the surface with which to challenge models at the GCM scale, and in their land-surface component, INCOMPASS also instituted a network of 8 flux towers across India to determine surface fluxes using modern eddy-covariance techniques. The flux towers are still operating at the time of writing and will provide the first freely available resource for fluxes with high accuracy.

### 5.1 Emerging results

In a study of climatological data, INCOMPASS has already established the key role played by a dry intrusion, retreating to the northwest of India while being eroded from beneath, in modulating the monsoon progression across the country (Parker et al., 2016). That work arose from ideas formulated during the first flight-planning exercises for INCOMPASS (Willetts et al., 2017b). Parker et al. (2016) hypothesized that the onset progression in part relates to moistening of the free troposphere at and below the freezing level by shallow clouds; there is also the suggestion that moistening of the soils ahead of the progressing monsoon, by light showers, will further aid its advancement. INCOMPASS modelling was then used to reinforce these ideas: Menon et al. (2018) have demonstrated, using initialized model data, that detrainment processes in shallow clouds do indeed act to moisten the column near the freezing level, pre-conditioning the column for subsequent deep convection. The field measurements obtained from our transit flights and described here in Section 4 support these general ideas about the onset.

Resulting from our mission at the southern base in Bengaluru, Fletcher et al. (2019) have suggested the role of another type of dry intrusion interacting with Western Ghats rainfall and regimes of onshore and offshore convection on an intraseasonal basis. Similarly, our observations of the July 2016 monsoon depression, including in flight B974, suggested that

dry intrusions are also implicated in monsoon depressions, leading to mixing of moist and dry air masses. Motivated by this, Fletcher et al. (2018) have demonstrated that 40% of depressions over India interact with intrusions of dry desert air masses, reducing rainfall in the rainiest part of the storm. It remains to be seen what model configurations are needed to capture such characteristics.

The modulation of cloud radiative forcing by synoptic activity in the monsoon such as the 2016 depression has also been measured in INCOMPASS. Using radiosonde analysis at Kanpur, George et al. (2018) noted that during the passage of the depression, cloud bases were lower and cloud depths greater; in general cloud radiative forcing in the shortwave was found to dominate that in the longwave for both surface and top of atmosphere (TOA), providing a net cooling effect.

Meanwhile at the surface, Bhat et al. (2019) have given a comprehensive overview of the diurnal cycle of surface fluxes at flux towers across India and their seasonal cycle. These demonstrate the importance of agricultural practices as well as meteorology in determining the partition between sensible and latent heat fluxes. At smaller scales, Barton et al. (2019) have demonstrated that gradients in soil moisture, whether caused by antecedent rainfall or irrigation practices, lead to mesoscale convergence patterns that can initiate storms. Finally, using the IIT Kanpur flux tower observations, Chakraborty et al. (2019) found that the NOAH land-surface model significantly underestimates the latent heat flux over the region during the monsoon onset period, which was partly addressed by improving the vegetation parametrization in the model.

Further work in this Special Collection will document the modelling capability implemented at the Met Office and NCMRWF for forecasting the 2016 monsoon. The utility of additional observations derived from the field campaign as additional inputs in the model assimilation scheme will be assessed. In addition it will examine detailed observations and modelling of the monsoon depression over northern India in July 2016. Finally, flux tower outputs will be compared with representations of the land surface from the JULES models to determine which land surface types yield the largest errors.

## 5.2 Outlook

The results generated so far in INCOMPASS have led to generation of new hypotheses and motivate further work.

A key observation made from flights from Bengaluru was of the co-existence of convection at multiple stages of development and the predominance of congestus clouds. Despite their informal nature, such visual observations are valuable for informing our modellers what they need to be aiming for when developing convection schemes. There is thus an urgent need to fully characterise the convective lifecycle, given its poor representation in models. This encompasses the diurnal cycle of convection, and the response of that diurnal cycle to forcing, whether arising from features at the mesoscale, synoptic or large scales. For example, how do passing features such as convergence lines, monsoon depressions or tropical

waves modify monsoon convection? This also applies to forcing from the surface, so a key hypothesis to be tested is how the widespread irrigation observed from our flights in the Ganges basin affects mesoscale circulations and storm development in nearby non-irrigated regions.

A general question surrounding the monsoon onset progression is to what extent it can be regarded as a subcontinental-scale representation of the convective lifecycle. Do the same processes that pervade in the monsoon convective lifecycle on a day-by-day basis also manifest in the onset? How much does wetting of the surface from light and intermittent pre-monsoon rains contribute to the progression?

Finally, of utmost importance to India, especially in agriculture, is the forecasting of monsoon intraseasonal variability. The INCOMPASS work of Fletcher et al. (2019), and the earlier work of Bhat (2006) in the presence of a mid-level dry intrusion in the July 2002 monsoon drought, motivate questions as to the generality of such instances. A key hypothesis is thus that intraseasonal dry intrusions play a key role in reducing rainfall over India in response to forcing from boreal summer intraseasonal variability at the large scale. Detailed modelling could be used to determine whether the dry intrusion is a passive response to large-scale forcing or plays a more active role in monsoon breaks.

We conclude that the general approach of INCOMPASS appears to be being borne out: we do find significant coupling between the land and atmosphere, and the physics and dynamics of the monsoon, on a variety of scales. Our observations from the INCOMPASS field campaign have opened a window on this to serve as a starting point. When combined with long-term data from remote-sensing and reanalysis products we endeavour to understand remaining issues in the monsoon in future research.

### 5.3 Data availability

New observations collected by the INCOMPASS field campaign are being made freely available. Flight data and Kanpur radiosonde launches are already freely available, upon registration, from the UK Centre for Environmental Data Analysis (CEDA) at <http://catalogue.ceda.ac.uk/uuid/1873b605e2a74cac8b4f5d12593e54fc>. Outputs from flux towers are available from the Environmental Information Data Centre at <https://doi.org/10.5285/78c64025-1f8d-431c-bdeb-e69a5877d2ed> and <https://doi.org/10.5285/c5e72461-c61f-4800-8bbf-95c85f74c416>. Further data will be added in due course.

### Acknowledgements

INCOMPASS was jointly funded in the UK and India by the Natural Environment Research Council (grants NE/L01386X/1, NE/L013843/1, NE/L013819/1 & NE/P003117/1) and Ministry of Earth Sciences, under the Monsoon Mission, respectively. D. J. Parker was also supported by a Royal Society Wolfson Research Merit Award. G. M. Martin was supported by the Met Office Hadley Centre Climate Programme funded by BEIS and Defra. Airborne

data was obtained using the BAe-146-301 Atmospheric Research Aircraft flown by Directflight Ltd. (now Airtask Ltd.) and managed by the Facility for Airborne Atmospheric Measurements (FAAM), which is a joint entity of the Natural Environment Research Council (NERC) and the Met Office. The authors gratefully acknowledge those others involved in the deployment of the aircraft to India: M. Rajeevan (MoES Secretary), Parvinder Maini, RS Maheshkumar (MoES) and N. Garnett (NERC). We thank ISRO for allowing the placement of eddy covariance sensors on its AMS masts. We further thank the Editors and two anonymous reviewers for their comments on this work.

## References

- Aranami, K., Davies, T. and Wood, N. (2015) A mass restoration scheme for limited-area models with semi-Lagrangian advection. *Quarterly Journal of the Royal Meteorological Society*, **141**, 1795–1803.
- Barton, E., Taylor, C. M., Parker, D. J., Turner, A. G., Belušić, D., Boeing, S., Brooke, J. K., Harlow, R. C., Harris, P. P., Hunt, K., Jayakumar, A. and Mitra, A. K. (2019) A case study of land-atmosphere coupling during monsoon onset in northern India. *Quarterly Journal of the Royal Meteorological Society*, **published online**. URL: <https://doi.org/10.1002/qj.3538>.
- Bhat, G., Gadgil, S., Kumar, P., Kalsi, S., Madhusoodanan, P., Murty, V., Rao, C., Babu, V., Rao, L., Rao, R., Ravichandran, M., Reddy, K., Rao, P., Sengupta, D., Sikka, D., Swain, J. and Vinayachandran, P. (2001) BOBMEX: The Bay of Bengal Monsoon Experiment. *Bulletin of the American Meteorological Society*, **82**, 2217–2243.
- Bhat, G. S. (2006) The Indian drought of 2002—a sub-seasonal phenomenon. *Quarterly Journal of the Royal Meteorological Scoiety*, **132**, 2583–2602.
- Bhat, G. S., Morrison, R., Taylor, C. M., Bhattacharya, B. K., Paleri, S., Desai, D., Evans, J. G., Pattnaik, S., Sekhar, M., Nigam, R., Sattar, A., Angadi, S. S., Kacha, D., Patidar, A., N., T. S., Krishna, K. V. M. and Sisodiya, A. (2019) Spatial and temporal variability in energy and water vapor fluxes across the Indian subcontinent. *Quarterly Journal of the Royal Meteorological Society*, **submitted**.
- Bhat, G. S. and Narasimha, R. (2007) Indian summer monsoon experiments. *Current Science*, **93**, 153–164.
- Boos, W. R. and Kuang, Z. (2010) Dominant control of the South Asian monsoon by orographic insulation versus plateau heating. *Nature*, **463**, 218–U102.
- Brooks, J., Allan, J. D., Williams, P. I., Liu, D., Fox, C., Haywood, J., Langridge, J. M., Highwood, E. J., Kompalli, S. K., O’Sullivan, D., Babu, S. S., Satheesh, S. K., Turner, A. G. and Coe, H. (2019) Vertical and horizontal distribution of submicron aerosol chemical composition and physical characteristics across northern India during the pre-monsoon and monsoon seasons. *Atmospheric Chemistry and Physics*, **19**, 5615–5634.

- Chakraborty, T., Sarangi, C., Krishnan, M., Tripathi, S. N., Morrison, R. and Evans, J. (2019) Biases in model-simulated surface energy fluxes during the Indian monsoon onset period. *Boundary-Layer Meteorology*, **170**, 323–348.
- Challinor, A. J., Slingo, J. M., Turner, A. G. and Wheeler, T. (2006) Indian Monsoon: Contribution to the Stern Review. In *Stern Review on the Economics of Climate Change*. HM Treasury.
- Dee, D. P., Uppala, S. M., Simmons, A. J. and et al. (2011) The ERA-Interim reanalysis: configuration and performance of the data assimilation system. *Quarterly Journal of the Royal Meteorological Society*, **137**, 553–597.
- Errico, R. M., Yang, R., Masutani, M. and Woollen, J. S. (2007) The estimation of analysis error characteristics using an observation systems simulation experiment. *Meteorologische Zeitschrift*, **16**, 695–708.
- Evans, J. G., Ward, H. C., Blake, J. R., Hewitt, E. J., Morrison, R., Fry, M., Ball, L. A., Doughty, L. C., Libre, J. W., Hitt, O. E., Rylett, D., Ellis, R. J., Warwick, A. C., Brooks, M., Parkes, M. A., Wright, G. M. H., Singer, A. C., Boorman, D. B. and Jenkins, A. (2016) Soil water content in southern England derived from a cosmic-ray soil moisture observing system – COSMOS-UK. *Hydrological Processes*, **30**, 4987–4999.
- Fielder, L. and Bakan, S. (1997) Interferometric measurements of sea surface temperature and emissivity. *Deutsche Hydrografische Zeitschrift*, **49**, 357–365.
- Fletcher, J. K., Parker, D. J., Hunt, K. M. R., Vishwanathan, G. and Govindankutty, M. (2018) The Interaction of Indian Monsoon Depressions with Northwesterly Midlevel Dry Intrusions. *Monthly Weather Review*, **146**, 679–693.
- Fletcher, J. K., Parker, D. J., Turner, A. G., Menon, A., Martin, G. M., Birch, C. E., Mitra, A. K., Mrudula, G., Hunt, K. M. R., Taylor, C. M., Houze, R. A., Brodzik, S. R. and Bhat, G. S. (2019) The dynamic and thermodynamic structure of the monsoon over southern India: New observations from the INCOMPASS IOP. *Quarterly Journal of the Royal Meteorological Society*, **published online**. URL: <https://doi.org/10.1002/qj.3439>.
- Gadgil, S. (2018) The monsoon system: Land–sea breeze or the ITCZ? *Journal of Earth System Sciences*, **127**.
- Gadgil, S. and Gadgil, S. (2006) The Indian Monsoon, GDP and Agriculture. *Economic and Political Weekly*, **41**, 4887–4895.
- George, G., Sarangi, C., Tripathi, S. N., Chakraborty, T. and Turner, A. (2018) Vertical Structure and Radiative Forcing of Monsoon Clouds Over Kanpur During the 2016 INCOMPASS Field Campaign. *Journal of Geophysical Research-Atmospheres*, **123**, 2152–2174.
- Houze, R. and Churchill, D. (1987) Mesoscale Organization and Cloud Microphysics in a Bay of Bengal Depression. *Journal of the Atmospheric Sciences*, **44**, 1845–1867.

Hunt, K. M. R., Turner, A. G., Inness, P. M., Parker, D. E. and Levine, R. C. (2016a) On the Structure and Dynamics of Indian Monsoon Depressions. *Monthly Weather Review*, **144**, 3391–3416.

Hunt, K. M. R., Turner, A. G. and Parker, D. E. (2016b) The spatiotemporal structure of precipitation in Indian monsoon depressions. *Quarterly Journal of the Royal Meteorological Society*, **142**, 3195–3210.

Jayakumar, A., Abel, S. J., Turner, A. G., Mohandas, S., Sethunath, J., O’Sullivan, D. and Rajagopal, E. N. (2019) Performance of the NCMRWF convection-permitting model during contrasting monsoon phases of 2016 INCOMPASS field campaign. *Quarterly Journal of the Royal Meteorological Society*, submitted.

Jensen, M. P., Holdridge, D. J., Survo, P., Lehtinen, R., Baxter, S., Toto, T. and Johnson, K. L. (2016) Comparison of Vaisala radiosondes RS41 and RS92 at the ARM Southern Great Plains site. *Atmospheric Measurement Techniques*, **9**, 3115–3129.

Kohli, M., Schron, M., Zreda, M., Schmidt, U., Dietrich, P. and Zacharias, S. (2015) Footprint characteristics revised for field-scale soil moisture monitoring with cosmic-ray neutrons. *Water Resources Research*, **51**, 5772–5790.

Krishnamurti, T. N., Simon, A., Thomas, A., Mishra, A. K., Sikka, D., Niyogi, D., Chakraborty, A. and Li, L. (2012) Modeling of forecast sensitivity on the March of monsoon isochorones from Kerala to New Delhi: the first 25 days. *Journal of the Atmospheric Science*, **69**, 2465–2487.

Li, C. and Yanai, M. (1996) The onset and interannual variability of the Asian summer monsoon in relation to land sea thermal contrast. *Journal of Climate*, **9**, 358–375.

Liu, D., Flynn, M., Gysel, M., Targino, A., Crawford, I., Bower, K., Choularton, T., Jurányi, Z., Steinbacher, M., Hüglin, C. and Curtius, J. (2010) Single particle characterization of black carbon aerosols at a tropospheric alpine site in Switzerland. *Atmospheric Chemistry and Physics*, **10**, 7389–7407.

Mamgain, A., Rajagopal, E. N., Mitra, A. K. A. and Webster, S. (2018) Short-Range Prediction of Monsoon Precipitation by NCMRWF Regional Unified Model with Explicit Convection. *Pure and Applied Geophysics*, **175**, 1197–1218.

Mapes, B. E. and Zuidema, P. (1996) Radiative-Dynamical Consequences of Dry Tongues in the Tropical Troposphere. *Journal of the Atmospheric Sciences*, **53**, 620–639.

Marenco, F., Amiridis, V., Marinou, E., Tsekeli, A. and Pelon, J. (2014) Airborne verification of CALIPSO products over the Amazon: a case study of daytime observations in a complex atmospheric scene. *Atmospheric Chemistry and Physics*, **14**, 11871–11881.

Marenco, F., Johnson, B., Turnbull, K., Newman, S., Haywood, J., Webster, H. and Ricketts, H. (2011) Airborne Lidar Observations of the 2010 Eyjafjallajökull volcanic ash plume. *Journal of Geophysical Research - Atmospheres*, **116**, 1–15.

Martin, G. M., Brooks, M. E., Johnson, B., Milton, S. F., Webster, S., Jayakumar, A., Mitra, A., Rajan, D. and Hunt, K. M. R. (2019) Forecasting the monsoon on daily to seasonal timescales in support of a field campaign. *Quarterly Journal of the Royal Meteorological Society*, **published online**. URL: <https://doi.org/10.1002/qj.3620>.

Martin, G. M., Klingaman, N. P. and Moise, A. F. (2017) Connecting spatial and temporal scales of tropical precipitation in observations and the MetUM-GA6. *Geoscientific Model Development*, **10**, 105–126.

Martin, G. M., Milton, S. F., Senior, C. A., Brooks, M. E., Ineson, S., Reichler, T. and Kim, J. (2010) Analysis and Reduction of Systematic Errors through a Seamless Approach to Modeling Weather and Climate. *Journal of Climate*, **23**, 5933–5957.

Menon, A., Turner, A. G., Martin, G. M. and MacLachlan, C. (2018) Modelling the moistening of the free troposphere during the northwestward progression of Indian monsoon onset. *Quarterly Journal of the Royal Meteorological Society*, **144**, 1152–1168.

Mitra, A. K., Bohra, A. K., Rajeevan, M. N. and Krishnamurti, T. N. (2009) Daily Indian Precipitation Analysis Formed from a Merge of Rain-Gauge Data with the TRMM TMPA Satellite-Derived Rainfall Estimates. *Journal of the Meteorological Society of Japan*, **87A**, 265–279.

Mitra, A. K., Momin, I. M., Rajagopal, E. N., Basu, S., Rajeevan, M. N. and Krishnamurti, T. N. (2013) Gridded daily Indian monsoon rainfall for 14 seasons: Merged TRMM and IMD gauge analyzed values. *Journal of Earth System Science*, **122**, 1173–1182.

Molnar, P., Boos, W. R. and Battisti, D. S. (2010) Orographic Controls on Climate and Paleoclimate of Asia: Thermal and Mechanical Roles for the Tibetan Plateau. *Annual Review of Earth and Planetary Sciences*, **38**, 77–102.

Montzka, C., Bogena, H. R., Zreda, M., Monerris, A., Morrison, R., Muddu, S. and Vereecken, H. (2017) Validation of Spaceborne and Modelled Surface Soil Moisture Products with Cosmic-Ray Neutron Probes. *Remote Sensing*, **9**, 103.

Morrison, R., Angadi, S. S., Cooper, H. M., Evans, J., Rees, G., Sekhar, M., Taylor, C., Tripathi, S. N. and Turner, A. G. (2019a) High temporal resolution meteorology and soil physics observations from INCOMPASS land surface stations in India, 2016 to 2018. NERC Environmental Information Data Centre. URL: <https://doi.org/10.5285/c5e72461-c61f-4800-8bbf-95c85f74c416>.

Morrison, R., Angadi, S. S., Cooper, H. M., Evans, J. G., Rees, G., Sekhar, M., Taylor, C., Tripathi, S. N. and Turner, A. G. (2019b) Energy and carbon dioxide fluxes, meteorology and soil physics observed at INCOMPASS land surface stations in India, 2016 to 2017. NERC Environmental Information Data Centre. URL: <https://doi.org/10.5285/78c64025-1f8d-431c-bdeb-e69a5877d2ed>.

- Newman, S. M., Smith, J. A., Glew, M. D., Rogers, S. M. and Taylor, J. P. (2005) Temperature and salinity dependence of sea surface emissivity in the thermal infrared. *Quarterly Journal of the Royal Meteorological Society*, **131**, 2539–2557.
- Parker, D. J., Willetts, P., Birch, C., Turner, A. G., Marsham, J. H., Taylor, C. M., Kolusu, S. and Martin, G. M. (2016) The interaction of moist convection and mid-level dry air in the advance of the onset of the Indian monsoon. *Quarterly Journal of the Royal Meteorological Society*, **142**, 2256–2272.
- Parsons, D. P., Redelsperger, J.-L. and Yoneyama, K. (2000) The evolution of the tropical western Pacific atmosphere-ocean system following the arrival of a dry intrusion. *Quarterly Journal of the Royal Meteorological Society*, **126**, 517–548.
- Petersen, G. N. and Renfrew, I. A. (2009) Aircraft-based observations of air-sea fluxes over Denmark Strait and the Irminger Sea during high wind speed conditions. *Quarterly Journal of the Royal Meteorological Society*, **135**, 2030–2045.
- Renfrew, I. A., Petersen, G. N., Sproson, D. A. J., Moore, G. W. K., Adiwidjaja, H., Zhang, S. and North, R. (2009) A comparison of aircraft-based surface-layer observations over Denmark Strait and the Irminger Sea with meteorological analyses and QuikSCAT winds. *Quarterly Journal of the Royal Meteorological Society*, **135**, 2046–2066.
- Ryder, C., McQuaid, J., Flamant, C., Rosenberg, P., Washington, R., Brindley, H., Highwood, E., Marsham, J., Parker, D., Todd, M., Banks, J., Brooke, J., Engelstaedter, S., Estelles, V., Formenti, P., Garcia-Carreras, L., Kocha, C., Marenco, F., Sodemann, H., Allen, C., Bourdon, A., Bart, M., Cavazos-Guerra, C., Chevaillier, S., Crosier, J., Darbyshire, E., Dean, A., Dorsey, J., Kent, J., O'Sullivan, D., Schepanski, K., Szpek, K., Trembath, J. and Woolley, A. (2015) Advances in understanding mineral dust and boundary layer processes over the Sahara from Fennec aircraft observations. *Atmospheric Chemistry and Physics*, **15**, 8479–8520.
- Saha, K., Sanders, F. and Shukla, J. (1981) Westward Propagating Predecessors of Monsoon Depressions. *Monthly Weather Review*, **109**, 330–343.
- Sandeep, A., Mitra, A. K., Turner, A. G., Rajagopal, E. N., Jyothi, K. A., Bhat, G. S. and Jayakumar, A. (2019) Inter-comparison of large-scale weather in the NCMRWF NWP model and FAAM aircraft measurements during the 2016 INCOMPASS field campaign. *Quarterly Journal of the Royal Meteorological Society*, submitted.
- Sperber, K. R., Annamalai, H., Kang, I. S., Kitoh, A., Moise, A., Turner, A., Wang, B. and Zhou, T. (2013) The Asian summer monsoon: an intercomparison of CMIP5 vs. CMIP3 simulations of the late 20th century. *Climate Dynamics*, **41**, 2711–2744.
- Stephens, M., Turner, N. and Sandberg, J. (2003) Particle Identification by Laser-Induced Incandescence in a Solid-State Laser Cavity. *Applied Optics*, **42**, 3726–3736.

- Stirling, J. and Stratton, R. A. (2012) Entrainment processes in the diurnal cycle of deep convection over land. *Quarterly Journal of the Royal Meteorological Society*, **138**, 1135–1149.
- Taylor, C. M., Gounou, A., Guichard, F., Harris, P. P., Ellis, R. J., Couvreux, F. and De Kauwe, M. (2011) Frequency of Sahelian storm initiation enhanced over mesoscale soil-moisture patterns. *Nature Geoscience*, **4**, 430–433.
- Turner, A. G. and Annamalai, H. (2012) Climate change and the South Asian summer monsoon. *Nature Climate Change*, **2**, 587–595.
- Vance, A. K., Abel, S. J., Cotton, R. J. and Woolley, A. M. (2015) Performance of WVSS-II hygrometers on the FAAM research aircraft. *Atmospheric Measurement Techniques*, **8**, 1617–1625.
- Vernekar, K. G., Sinha, S., Sadani, L., Sivaramakrishnan, S., Parasnis, S. S., Mohan, B., Dharmaraj, S., Patil, M. N., Pillai, J. S., Murthy, B. S., Debaje, S. B. and Bagavathsingh, A. (2003). *Boundary-Layer Meteorology*, **106**, 561–572.
- Vinayachandran, P. N., Matthews, A. J., Vijay Kumar, K., Sanchez-Franks, A., Thushara, V., George, J., Vijith, V., Webber, B. G. M., Queste, B. Y., Roy, R., Sarkar, A., Baranowski, D. B., Bhat, G. S., Klingaman, N. P., Peatman, S. C., Parida, C., Heywood, K. J., Hall, R., King, B., Kent, E. C., Nayak, A. A., Neema, C. P., Amol, P., Lotliker, A., Kankonkar, A., Gracias, D. G., Vernekar, S., Souza, A. C. D., Valluvan, G., Pargaonkar, S. M., Dinesh, K., Giddings, J. and Joshi, M. (2018) BoBBLE (Bay of Bengal Boundary Layer Experiment): Ocean–atmosphere interaction and its impact on the South Asian monsoon. *Bulletin of the American Meteorological Society*, **99**, 1569–1587.
- Volonté, A., Turner, A. G. and Menon, A. (2019) Airmass analysis of the processes driving the progression of the Indian summer monsoon. *Quarterly Journal of the Royal Meteorological Society*, **submitted**.
- Walters, D., Boutle, I., Brooks, M., Melvin, T., Stratton, R., Vosper, S., Wells, H., Williams, K., Wood, N., Allen, T., Bushell, A., Copsey, D., Earnshaw, P., Edwards, J., Gross, M., Hardiman, S., Harris, C., Heming, J., Klingaman, N., Levine, R., Manners, J., Martin, G., Milton, S., Mittermaier, M., Morcrette, C., Riddick, T., Roberts, M., Sanchez, C., Selwood, P., Stirling, A., Smith, C., Suri, D., Tennant, W., Vidale, P. L., Wilkinson, J., Willett, M., Woolnough, S. and Xavier, P. (2017) The Met Office Unified Model Global Atmosphere 6.0/6.1 and JULES Global Land 6.0/6.1 configurations. *Geoscientific Model Development*, **10**, 1487–1520.
- Willett, P. D., Marsham, J. H., Birch, C. E., Parker, D. J., Webster, S. and Petch, J. (2017a) Moist convection and its upscale effects in simulations of the Indian monsoon with explicit and parametrized convection. *Quarterly Journal of the Royal Meteorological Society*, **143**, 1073–1085.

Willetts, P. D., Turner, A. G., Martin, G. M., Mrudula, G., Hunt, K. M. R., Parker, D. J., Taylor, C. M., Birch, C. E., Mitra, A. K., Heming, J. T. and Brooks, M. E. (2017b) The 2015 Indian summer monsoon onset - phenomena, forecasting and research flight planning. *Weather*, **72**, 168–175.

Wilson, S. H. S., Atkinson, N. C. and Smith, J. A. (1999) The development of an airborne infrared interferometer for meteorological sounding studies. *Journal of Atmospheric and Oceanic Technology*, **16**, 1912–1927.

Xavier, P. K., Marzin, C. and Goswami, B. N. (2007) An objective definition of the Indian summer monsoon season and a new perspective on the ENSO-monsoon relationship. *Quarterly Journal of the Royal Meteorological Society*, **133**, 749–764.

Zreda, M., Shuttleworth, W. J., Zeng, X., Zweck, C., Desilets, D., Franz, T. and Rosolem, R. (2012) COSMOS: the COsmic-ray Soil Moisture Observing System. *Hydrology and Earth System Science*, **16**, 4079–4099.

Figure 1 Mean sea-level pressure derived from ERA-Interim (units hPa) over June to August 1979–2012 (contours); also shown is the fraction of land equipped for irrigation (coloured shading) from the UN Food and Agriculture Organisation Global Map of Irrigation Areas v5 for 2005. Orography over 600m is shaded grey; the 3000m contour is shown in purple as an indicative outline the Tibetan plateau. The position of the Himalayas at the southern edge of the Tibetan Plateau are indicated, as are the Indo-Gangetic plains (IGP) of northern India, the Western Ghats mountains and the Arabian Sea and Bay of Bengal portions of the Indian Ocean.

Figure 2 Typical monsoon progression from May to July based on APHRODITE gauge rainfall at  $0.5^{\circ}$ -resolution, computed over 1951–2007 during the indicated week in: (a) mid-May; (b) mid-June; (c) mid-July. Units are  $\text{mm day}^{-1}$ . The closest onset isochrones in time are also shown for 20 May, 15 June, 15 July, respectively (filled black circles; the monsoon lying to the south and east of the isochrone), as provided by the India Meteorological Department (IMD). Surface soil moisture (% saturation) from the European Space Agency (ESA)-Climate Change Initiative (CCI) active product determined from satellite measurements over 2007–2016 is also shown for the same dates in (d-f) at  $0.5^{\circ}$ -resolution. Land areas shown white correspond to missing data/snow cover. Units are %.

Figure 3 Map of flights performed during the INCOMPASS field campaign, indicating longitude/latitude position in each case. Flights are grouped together by purpose (colour). The Lucknow and Bengaluru airports are also indicated.

Figure 4 Height-longitude cross section of flights undertaken from (a) Lucknow / northern base and (b) Bengaluru / southern base during the INCOMPASS field campaign. Flights are grouped together by colour, indicating their purpose as in Figure 3. Pressure height is taken from the aircraft's static pressure reading; approximate height above sea level is also given in km and hft (hectofeet), corresponding to aviation flight levels.

Figure 5 Example day-2 accumulated rainfall forecasts valid for 5 July 2016 in various versions of the NCUM at NCMRWF: (a) observations from the NCMRWF/IMD merged satellite and gauge product (Mitra et al., 2009, 2013); (b) global 17 km model; (c) 4 km LAM; (d) 1.5 km LAM. Units are cm/day.

Figure 6 Locations of all ground and upper-air stations employed by INCOMPASS: 8 eddy covariance flux tower installations (green triangles) and 19 IMD upper-air stations augmented with additional launches performed for INCOMPASS (red circles; for additional station details see Table 3; larger symbols indicate those providing data for Figure 13). Also shown are the location of supersites (blue filled stars) at Kanpur and Bhubaneswar and a further microwave radiometer (blue unfilled star) at Bhopal. See Table 2 for detailed locations of all ground instrumentation.

Figure 7 Diurnal variation of (a) sensible heat flux (SH); (b) latent heat flux (LH); (c) turbulent heat flux (where  $\text{THF}=\text{SH}+\text{LH}$ ), in which red and green refer to Jaiselmer and Samastipur, respectively; (d) SH versus LH at Jaiselmer; and (e) SH versus LH at Samastipur. Data is sampled over August 2016. Day-to-day variability is quantified by one-standard deviation error bars in (a) and (b) or dashed lines in (c). Units are  $\text{Wm}^{-2}$ . The time axes in panels (a)-(c) are expressed in terms of Indian Standard Time (IST).

Figure 8 Radiosonde launches achieved across the diurnal cycle (hours UTC) during the intensive observing period (IOP) from IIT Kanpur ( $26.52^{\circ}\text{N}$ ,  $80.23^{\circ}\text{E}$ ). Times marked with a double tick indicate where a second radiosonde was deployed followed a balloon or measurement failure.

Figure 9 Accumulated rainfall from 1 June to (a) 13 June 2016, date of southward transit flight B958 and (b) 28 June 2016, date of northward transit flight B967. Data are from the NCMRWF/IMD merged satellite and gauge product (Mitra et al., 2009, 2013). Units are mm. The flight tracks on each day are shown, terminating in the north at the Lucknow airbase and Bengaluru in the south. Also shown are the closest available IMD climatological positions of the monsoon advance to the flight dates (15 June and 1 July, respectively, black dots), as well as onset isochrones recorded in IMD charts for 2016 (14 June and 26 June, red line, again the closest available).

Figure 10 Surface changes between 13 June and 28 June 2016, based on a three-day centred mean in each case: (a) volumetric surface soil moisture (%) from the Advanced Microwave Scanning Radiometer 2 (AMSR2) satellite product; and (b) surface skin temperature (shading) and surface-air temperature (contours). Skin temperatures are generated from AMSR2 overpasses at 1330L; air temperatures (at 2m) are from ERA-Interim (Dee et al., 2011) (units are K). Each product is shown on its native grid. The route of transit flights B958 & B967 is shown in black, terminating in the north at Lucknow and Bengaluru in the south; red lines show the 2016 monsoon position as in Figure 9.

Figure 11 Latitude-height cross-sections of equivalent potential temperature ( $\theta_e$ ) for (a) 13 June and (b) 28 June 2016 from ERA-Interim analysis at 06Z, zonally averaged from 78–

81°E (shaded). Three-minute average of measurements from the southward and northward transit flights (B958 and B967, respectively) are overlaid (filled points). Units are K.

Figure 12 Tephigrams constructed from the upper-air station at Nagpur at 17:30L (12Z), ERA-Interim data at 06Z and the descending portion of flights in the vicinity of Nagpur on (a) 13 June / B958 and (b) 28 June / B967. Air temperature ( $T$ ) is represented by the red shades, while dewpoint temperature ( $T_d$ ) is shown in blue shades. Only the portion beneath  $\approx 350\text{hPa}$  is shown, consistent with the vertical position of the aircraft. For ease of reading, lines of constant mixing ratio and moist adiabats have been removed.

Figure 13 Tephigrams constructed from upper-air stations at (from south to north): (a,g) Bengaluru, (b,h) Hyderabad, (c,i) Nagpur, (d,j) Bhopal, (e,k) Gwalior and (f,l) Lucknow taken at 17:30L (12Z) on 13 June (left section; a-f) and 28 June (right section; g-l). The environment ( $T$ ) and dewpoint ( $T_d$ ) temperatures are shown in red and blue, respectively. As indicated on Figure 9, Bhopal and Gwalior lie to the west of the flight path. All data are high resolution (1s sampling) other than Nagpur, and Bengaluru on 28 June.

Table 1 Table of flight sorties performed during the INCOMPASS field campaign, listed in order of flight number. The aircraft operating base is listed, together with the primary scientific purpose of each flight and direction of operation from the base. Other features encountered are listed. Take-offs are specified in local time (UTC+5h30). Location coordinates for the two airports are given in the footer.

Date	Base	Flight ID	Take-off	Duration	Brief objective	Other points of interest
Sat 11 Jun	LKO	B956	0830L	4h30m	northern gradients; west; pre-monsoon	heat low, dust, irrigation
Sun 12 Jun	LKO	B957	0900L	4h30m	northern gradients; east; pre-monsoon	coast, forest
Mon 13 Jun	LKO	B958	1100L	4h30m	science transit to Bengaluru	meridional gradients
Tue 21 Jun	BLR	B959	1100L	4h30m	southern gradients; west; Arabian Sea	coast, orography
Wed 22 Jun	BLR	B960	1100L	4h00m	southern gradients; southeast; BoB	rain shadow, coast
Thu 23 Jun	BLR	B961	1100L	4h30m	southern gradients; west; Arabian Sea	coast, orography

Thu 23 Jun	BLR	B962	1700L	3h00m	southern gradients; west; Arabian Sea	coast, orography
Sat 25 Jun	BLR	B963	2130L	3h30m	southern gradients; west; Arabian Sea	coast, orography
Sun 26 Jun	BLR	B964	1100L	5h00m	southern gradients; west; Arabian Sea	coast, orography
Sun 26 Jun	BLR	B965	1700L	3h30m	southern gradients; west; Arabian Sea	coast, orography
Mon 27 Jun	BLR	B966	1100L	4h45m	southern gradients; southeast; BoB	coast, ship overpass
Tue 28 Jun	BLR	B967	1100L	5h00m	science transit to Lucknow	meridional gradients
Thu 30 Jun	LKO	B968	0900L	4h30m	northern gradients; west; mature monsoon	heat low, dust, irrigation
Sat 2 Jul	LKO	B969	0900L	4h30m	northern gradients; west; mature monsoon	heat low, dust, irrigation
Sun 3 Jul	LKO	B970	0900L	4h30m	northern gradients; west; mature monsoon	heat low, dust, irrigation
Mon 4 Jul	LKO	B971	0900L	4h30m	northern gradients; east; mature monsoon	coast, forest
Tue 5 Jul	LKO	B972	0900L	4h30m	northern gradients; west; mature monsoon	heat low, dust, irrigation
Wed 6 Jul	LKO	B973	0730L	4h30m	northern gradients; west;	heat low, dust, irrigation

					mature monsoon	
Thu 7 Jul	LKO	B974	1000L	4h00m	monsoon depression; south-west	
Sat 9 Jul	LKO	B975	1000L	4h30m	northern gradients; east; mature monsoon	coast, forest
Sun 10 Jul	LKO	B976	1000L	4h30m	northern gradients; west; mature monsoon	heat low, dust, irrigation
Mon 11 Jul	LKO	B977	1000L	1h00m	MoES demonstration flight; west	irrigation

LKO, Lucknow ( $26.76^{\circ}\text{N}$ ,  $80.88^{\circ}\text{E}$  & 123m above sea level); BLR, Bengaluru ( $12.95^{\circ}\text{N}$ ,  $77.67^{\circ}\text{E}$  & 888m above sea level); BoB, Bay of Bengal.

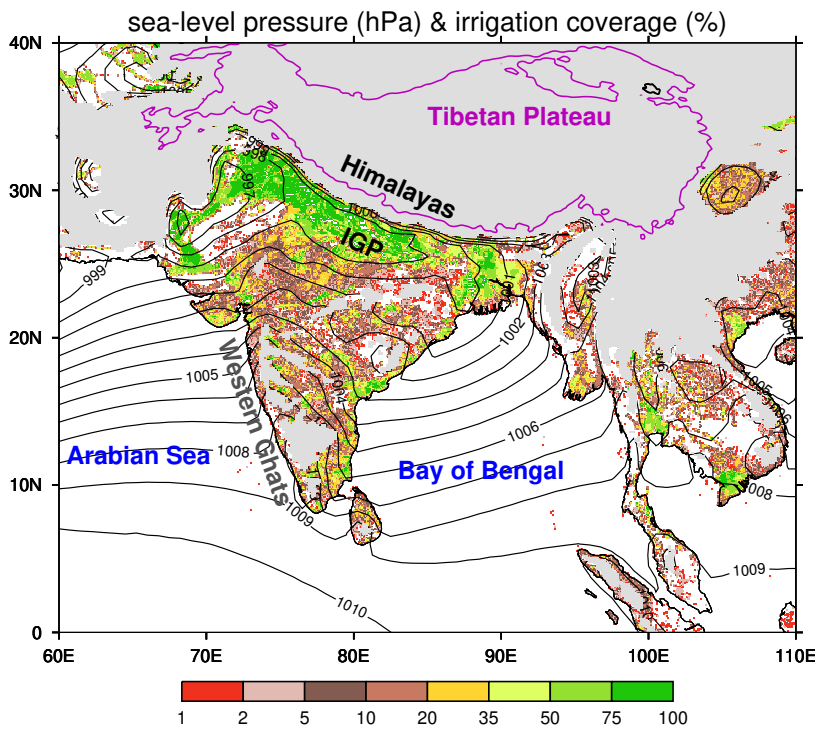
Table 2 Details of ground instrumentation installed or operated for INCOMPASS as depicted in Figure 6, including operational date. Upper-air stations (radiosondes) are listed separately in Table 3. See the subsections below for further information.

Instrument	Location	Lat. ( $^{\circ}\text{N}$ )	Lon. ( $^{\circ}\text{E}$ )	Alt. (m)	Start date	Notes
Flux tower	Bengaluru (Karnataka)	13.02	77.57	910	8 Jun 2016	forest/natural vegetation
	Berambadi (Karnataka)	11.76	76.59	870	9 Sep 2015	mixed agriculture
	Bhubaneswar (Odisha)	20.15	85.68	45	31 May 2016	natural vegetation
	Chandan/Jai salmer (Rajasthan)	26.99	71.34	196	4 Jun 2016	natural sewan grass
	Dharwad (Karnataka)	15.50	74.99	656	11 Feb 2016	agriculture
	Kanpur (Uttar Pradesh)	26.51	80.22	128	2 Jan 2016	grassland
	Nawagam/Kheda (Gujarat)	22.80	72.57	55	21 May 2016	agriculture (rice)
	Pusa/Samas tipur (Bihar)	26.00	85.67	39	16 Jun 2016	agriculture (wheat-rice)
Microwave	Bhopal (Madhya Pradesh)	23.23	77.42	527	30 Jun 2016	in IMD premises

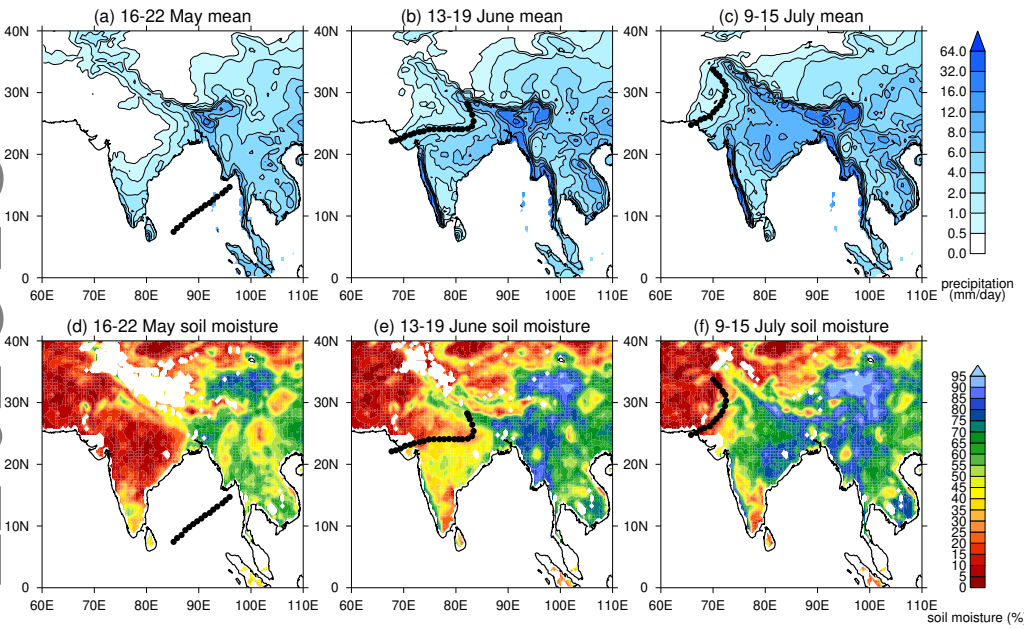
radiometer	Bhubaneswar (Odisha)	20.25	85.82	45	1 Jun 2016	IIT Bhubaneswar supersite
(MWR)	Kanpur (Uttar Pradesh)	26.52	80.23	182	23 Feb 2017	IIT Kanpur supersite
Ceilometer	Kanpur (Uttar Pradesh)	26.52	80.23	128	15 May 2016	IIT Kanpur supersite
Micro rain radar	Bhubaneswar (Odisha)	20.15	85.68	45	1 August 2016	IIT Bhubaneswar supersite

Table 3 Locations of IMD upper-air stations (19) featuring enhanced radiosonde balloon launches during the INCOMPASS Intensive Observing Period. The temporary launch site at IIT Kanpur is also listed. Stations marked with an asterisk (\*) are used in Figure 8.

Place	WMO ID	Latitude ( $^{\circ}$ N)	Longitude ( $^{\circ}$ E)	Altitude (m)	Notes
Ahmedabad	42647	23.07	72.63	55	
Aminidevi	43311	11.12	72.73	4	
Bangalore*	43295	12.97	77.58	920	=Bengaluru
Bhopal*	42667	23.28	77.35	523	
Bhubaneswar	42971	20.25	85.83	46	
Chennai	43279	13.00	80.18	16	
Gorakhpur	42379	26.75	83.37	77	
Gwalior*	42361	26.23	78.25	207	
Hyderabad*	43128	17.45	78.47	545	
Jodhpur	42339	26.30	73.02	224	
Kolkata	42809	22.65	88.45	5	
Lucknow*	42369	26.75	80.88	122	adjacent to airport base
Mangalore	43285	12.95	74.83	31	listed as Mangalore/Panambur
Mumbai	43003	19.12	72.85	14	Santacruz
Nagpur*	42867	21.10	79.05	308	
New Delhi	42182	28.58	77.20	267	
Patna	42492	25.60	85.10	60	
Port Blair	43333	11.67	92.72	79	
Trivandrum	43371	8.48	76.95	64	
Kanpur	-	26.52	80.23	126	IIT Kanpur supersite



**FIGURE 1** Mean sea-level pressure derived from ERA-Interim (units hPa) over June to August 1979–2012 (contours); also shown is the fraction of land equipped for irrigation (coloured shading) from the UN Food and Agriculture Organisation Global Map of Irrigation Areas v5 for 2005. Orography over 600m is shaded grey; the 3000m contour is shown in purple as an indicative outline the Tibetan plateau. The position of the Himalayas at the southern edge of the Tibetan Plateau are indicated, as are the Indo-Gangetic plains (IGP) of northern India, the Western Ghats mountains and the Arabian Sea and Bay of Bengal portions of the Indian Ocean.



**FIGURE 2** Typical monsoon progression from May to July based on APHRODITE gauge rainfall at  $0.5^{\circ}$ -resolution, computed over 1951-2007 during the indicated week in: (a) mid-May; (b) mid-June; (c) mid-July. Units are  $\text{mm day}^{-1}$ . The closest onset isochrones in time are also shown for 20 May, 15 June, 15 July, respectively (filled black circles; the monsoon lying to the south and east of the isochrone), as provided by the India Meteorological Department (IMD). Surface soil moisture (% saturation) from the European Space Agency (ESA)-Climate Change Initiative (CCI) active product determined from satellite measurements over 2007-2016 is also shown for the same dates in (d-f) at  $0.5^{\circ}$ -resolution. Land areas shown white correspond to missing data/snow cover. Units are %.

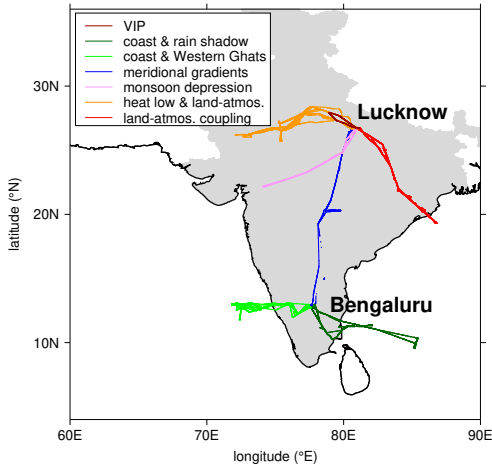


**FIGURE 3** Map of flights performed during the INCOMPASS field campaign, indicating longitude/latitude position in each case. Flights are grouped together by purpose (colour). The Lucknow and Bengaluru airports are also indicated.

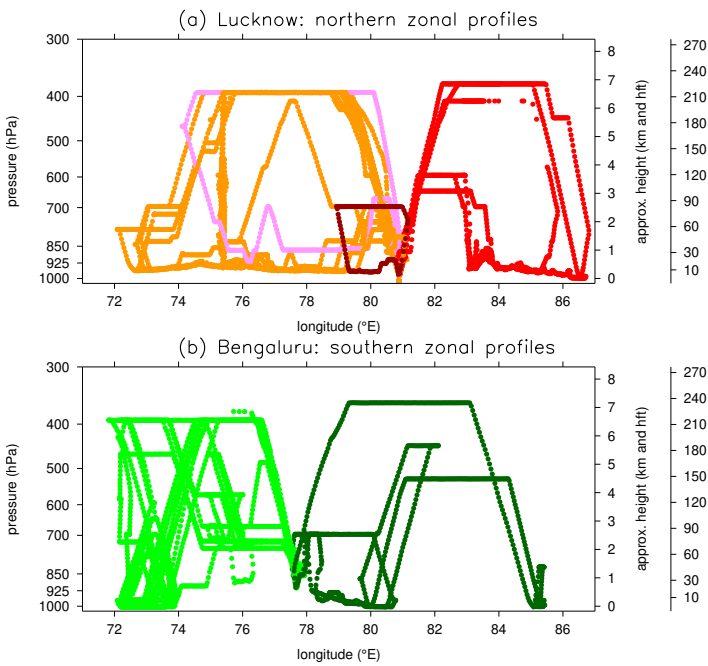


**FIGURE 4** Height-longitude cross section of flights undertaken from (a) Lucknow / northern base and (b) Bengaluru / southern base during the INCOMPASS field campaign. Flights are grouped together by colour, indicating their purpose as in Figure 3. Pressure height is taken from the aircraft's static pressure reading; approximate height above sea level is also given in km and hft (hectofeet), corresponding to aviation flight levels.

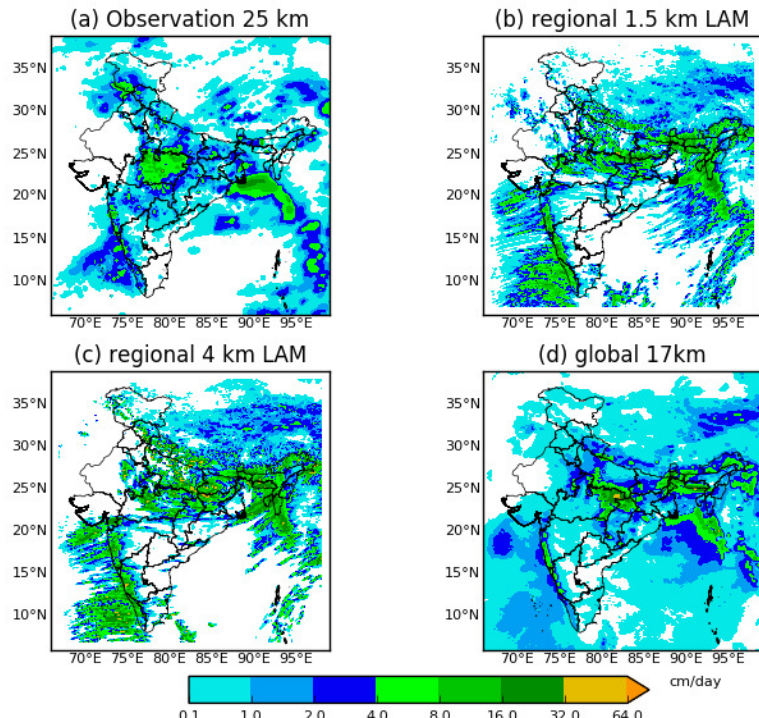


**FIGURE 5** Example day-2 accumulated rainfall forecasts valid for 5 July 2016 in various versions of the NCUM a NCMRWF: (a) observations from the NCMRWF/IMD merged satellite and gauge product (Mitra et al., 2009, 2013); (b) global 17 km model; (c) 4 km LAM; (d) 1.5 km LAM. Units are cm/day.

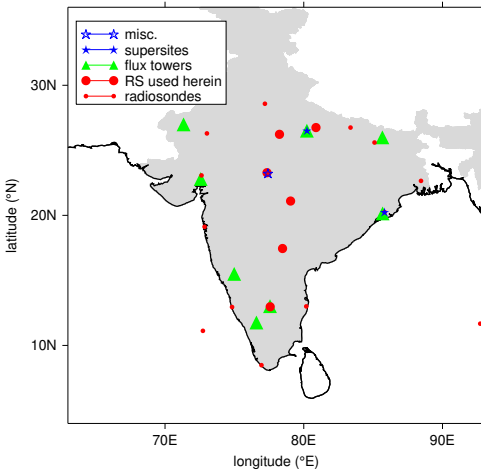


**FIGURE 6** Locations of all ground and upper-air stations employed by INCOMPASS: 8 eddy covariance flux tower installations (green triangles) and 19 IMD upper-air stations augmented with additional launches performed for INCOMPASS (red circles; for additional station details see Table 3; larger symbols indicate those providing data for Figure 13). Also shown are the location of supersites (blue filled stars) at Kanpur and Bhubaneswar and a further microwave radiometer (blue unfilled star) at Bhopal. See Table 2 for detailed locations of all ground instrumentation.

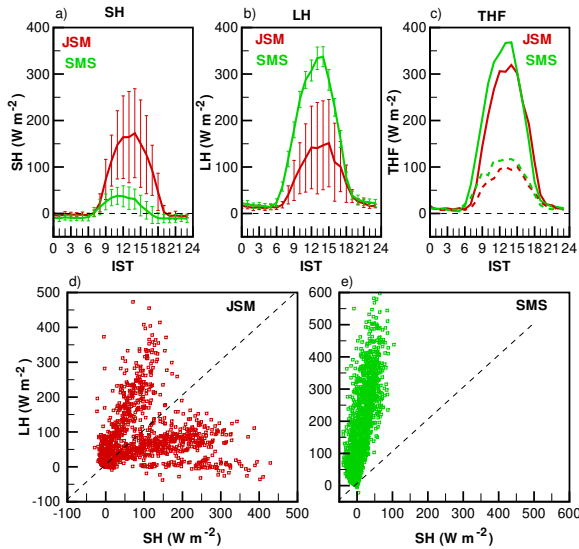


**FIGURE 7** Diurnal variation of (a) sensible heat flux (SH); (b) latent heat flux (LH); (c) turbulent heat flux (where  $THF = SH + LH$ ), in which red and green refer to Jaiselmer and Samastipur, respectively; (d) SH versus LH at Jaiselmer; and (e) SH versus LH at Samastipur. Data is sampled over August 2016. Day-to-day variability is quantified by one-standard deviation error bars in (a) and (b) or dashed lines in (c). Units are  $\text{Wm}^{-2}$ . The time axes in panels (a)-(c) are expressed in terms of Indian Standard Time (IST).

Date	Nominal launch time (UTC)								
	00	03	06	09	12	15	18	21	
05/07/2016	*	*	*	*	✓	*	✓	*	
06/07/2016	✓	*	✓	✓	✓	✓	✓	✓	
07/07/2016	✓	✓	✓	✓	*	✓	✓	✓	
08/07/2016	✓	✓	✓	✓	✓	✓	✓	✓	
09/07/2016	✓	✓	✓	✓	✓	✓	✓	✓	
10/07/2016	✓	✓	✓	✓	✓	✓	✓	✓	
11/07/2016	✓	✓	✓	✓	✓	✓	✓	✓	
12/07/2016	✓	✓	✓	✓	✓	✓	*	*	
13/07/2016	*	✓	✓	*	✓	*	*	*	
14/07/2016	*	✓	✓	✓	✓	✓	✓	*	
15/07/2016	✓	✓	✓	✓	✓	✓	*	✓	
16/07/2016	✓	✓	✓	✓	✓	✓	*	✓	
17/07/2016	✓	✓	*	✓	✓	✓	*	✓	
18/07/2016	✓	*	✓	✓	*	✓	*	✓	
19/07/2016	✓	✓	✓	*	✓	✓	*	✓	
20/07/2016	✓	✓	✓	✓	✓	✓	*	✓	
21/07/2016	✓	✓	*	✓	✓	✓	*	✓	
22/07/2016	✓	*	✓	✓	✓	✓	*	✓	
23/07/2016	✓	*	✓	*	✓	✓	*	✓	
24/07/2016	✓	*	✓	✓	✓	✓	*	✓	
25/07/2016	✓	*	✓	*	✓	✓	*	✓	
26/07/2016	✓	*	✓	✓	*	✓	*	✓	
27/07/2016	✓	*	✓	✓	✓	✓	✓	✓	
28/07/2016	✓	✓	✓	✓	*	*	*	*	

FIGURE 8 Radiosonde launches achieved across the diurnal cycle (hours UTC) during the intensive observing period (IOP) from IIT Kanpur ( $26.52^{\circ}\text{N}$ ,  $80.23^{\circ}\text{E}$ ). Times marked with a double tick indicate where a second radiosonde was deployed followed a balloon or measurement failure.

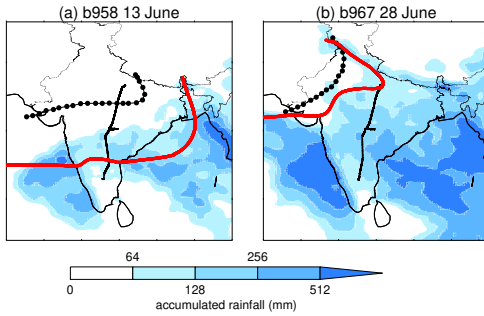


**FIGURE 9** Accumulated rainfall from 1 June to (a) 13 June 2016, date of southward transit flight B958 and (b) 28 June 2016, date of northward transit flight B967. Data are from the NCMRWF/IMD merged satellite and gauge product (Mitra et al., 2009, 2013). Units are mm. The flight tracks on each day are shown, terminating in the north at the Lucknow airbase and Bengaluru in the south. Also shown are the closest available IMD climatological positions of the monsoon advance to the flight dates (15 June and 1 July, respectively, black dots), as well as onset isochrones recorded in IMD charts for 2016 (14 June and 26 June, red line, again the closest available).

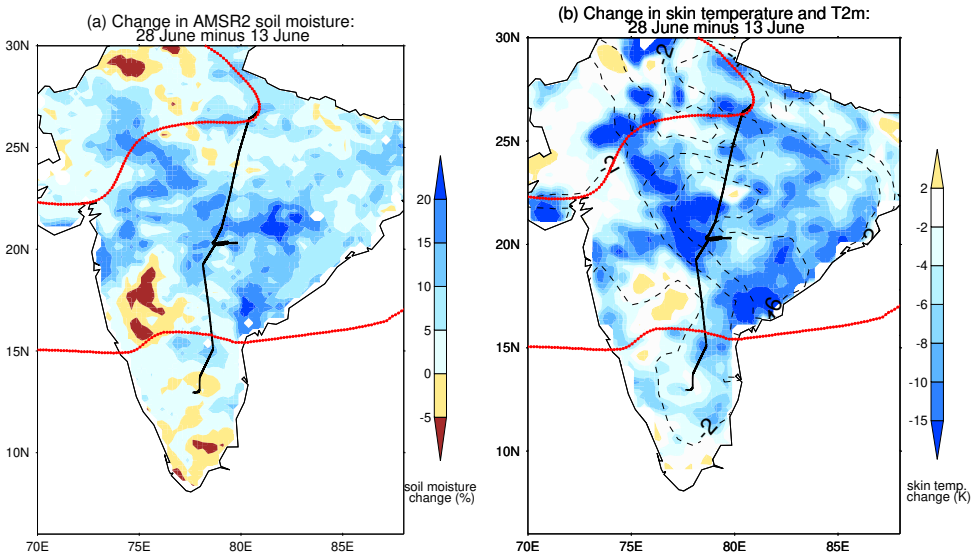


**FIGURE 10** Surface changes between 13 June and 28 June 2016, based on a three-day centred mean in each case: (a) volumetric surface soil moisture (%) from the Advanced Microwave Scanning Radiometer 2 (AMSR2) satellite product; and (b) surface skin temperature (shading) and surface-air temperature (contours). Skin temperatures are generated from AMSR2 overpasses at 1330L; air temperatures (at 2m) are from ERA-Interim (Dee et al., 2011) (units are K). Each product is shown on its native grid. The route of transit flights B958 & B967 is shown as black, terminating in the north at Lucknow and Bengaluru in the south; red lines show the 2016 monsoon position as in Figure 9.

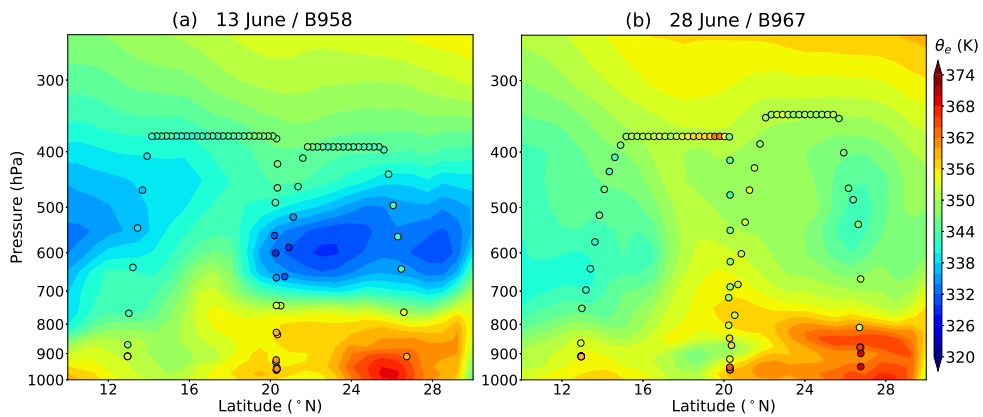
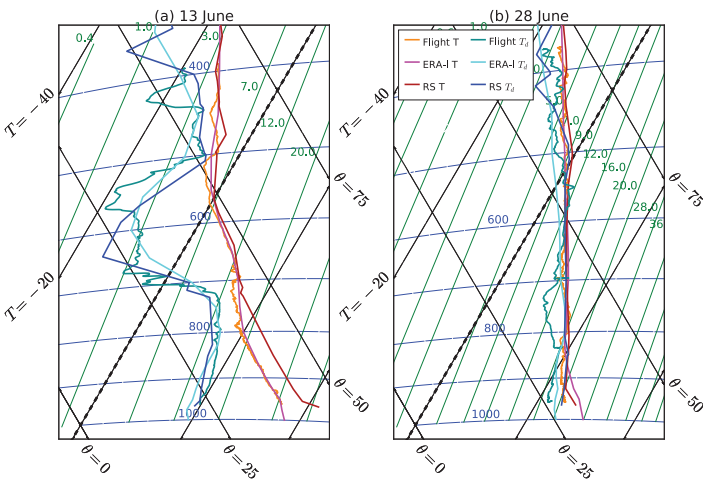
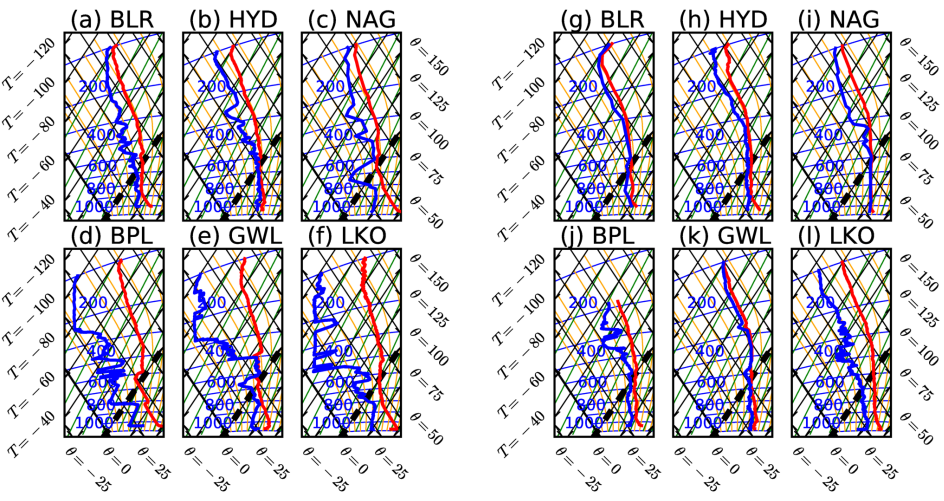


FIGURE 11 Latitude-height cross-sections of equivalent potential temperature ( $\theta_e$ ) for (a) 13 June and (b) 28 June 2016 from ERA-Interim analysis at 06Z, zonally averaged from 78–81 $^{\circ}$ E (shaded). Three-minute average of measurements from the southward and northward transit flights (B958 and B967, respectively) are overlaid (filled points). Units are K.



**FIGURE 12** Tephigrams constructed from the upper-air station at Nagpur at 17:30L (12Z), ERA-Interim data at 04Z and the descending portion of flights in the vicinity of Nagpur on (a) 13 June / B958 and (b) 28 June / B967. Air temperature ( $T$ ) is represented by the red shades, while dewpoint temperature ( $T_d$ ) is shown in blue shades. Only the portion beneath  $\approx 350\text{hPa}$  is shown, consistent with the vertical position of the aircraft. For ease of reading, lines of constant mixing ratio and moist adiabats have been removed.



**FIGURE 13** Tephigrams constructed from upper-air stations at (from south to north): (a,g) Bengaluru, (b,h) Hyderabad, (c,i) Nagpur, (d,j) Bhopal, (e,k) Gwalior and (f,l) Lucknow taken at 17:30L (12Z) on 13 June (left section; a-f) and 28 June (right section; g-l). The environment ( $T$ ) and dewpoint ( $T_d$ ) temperatures are shown in red and blue, respectively. As indicated on Figure 9, Bhopal and Gwalior lie to the west of the flight path. All data are high resolution (1s sampling) other than Nagpur, and Bengaluru on 28 June.